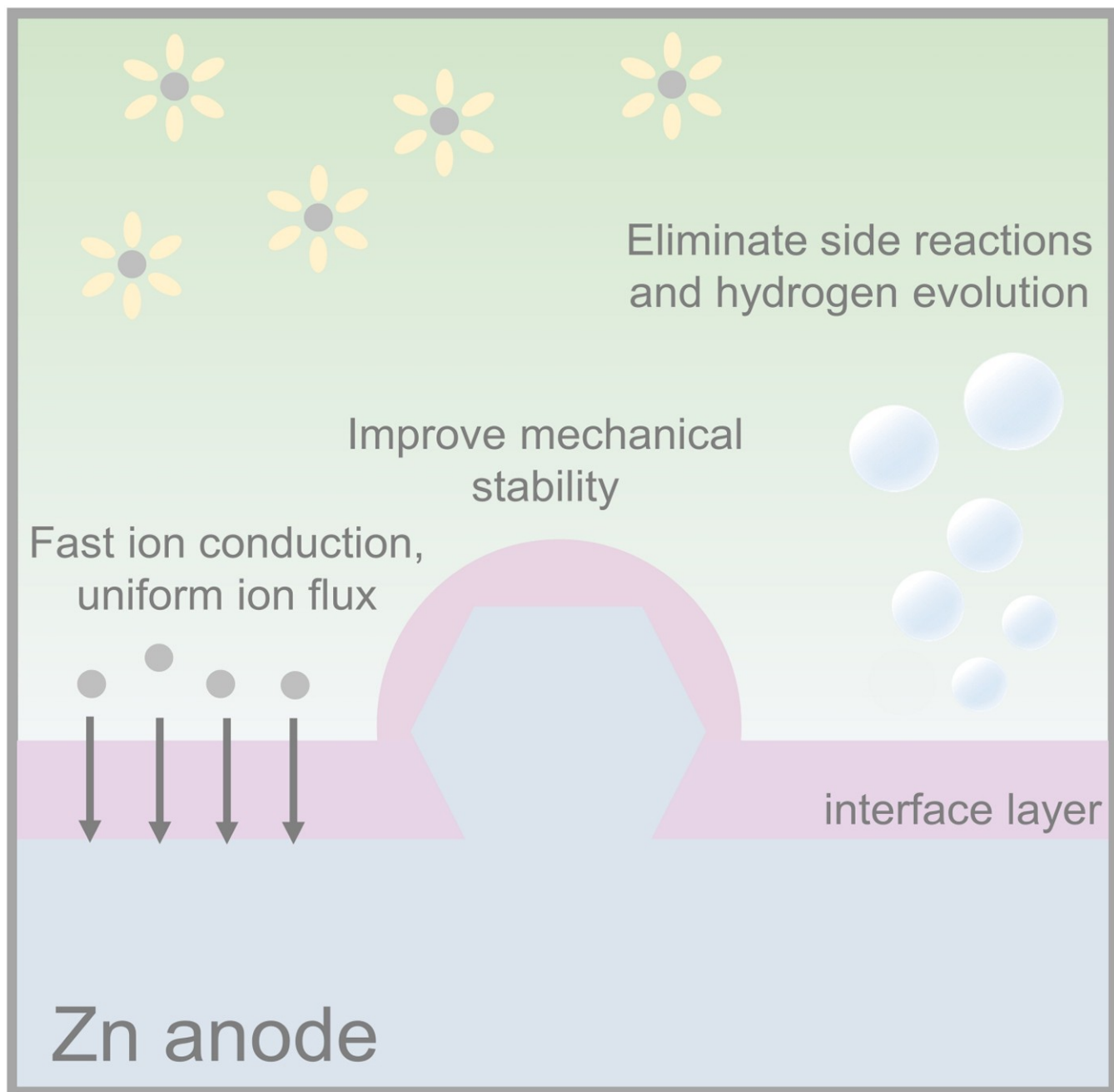


Guiding Principles for the Design of Artificial Interface Layer for Zinc Metal Anode

Zhikun Guo,^[a] Lishuang Fan,^{*[a]} Lijun Wu,^[b] Bingjiang Li,^[b] and Naiqing Zhang^{*[a]}



Zinc-ion battery has become a research hotspot in the energy storage field due to its low cost, high safety, and environmental friendliness. However, zinc as an anode has some problems such as dendrites and hydrogen evolution on the surface, which hinder the practical application of zinc. These problems are closely related to the plating and stripping behavior of zinc at the electrode interface. The construction of an artificial interface layer is one of the most direct and effective methods to protect

the zinc anode, which is helpful to improve the cycle life and utilization of the zinc anode. Here, we systematically review the progress and practical significance of artificial interfacial layers in terms of uniform ion transport, inhibition of side reactions and mechanical stability. Three design principles of the artificial interface layer are summarized to guide the further research, and to bring enlightenment for the construction of practical and efficient metal zinc anode.

1. Introduction

At present, traditional primary energy reserves are gradually depleted, and the direct combustion of fossil fuels leads to environmental problems. It is urgent to develop new energy which is green, clean and can replace traditional energy.^[1] However, these new energy sources, such as solar and wind, have the drawbacks of great volatility and intermittency, which limit their large-scale and long-term use. Lithium-ion batteries have dominated energy storage applications since their commercial development.^[2] However, lithium-ion batteries are facing with serious problems such as environmental pollution, poor safety and shortage of lithium resources, which are difficult to meet the market demand of large-scale energy storage industry in the future.^[3] Therefore, it is necessary to find new battery technologies based on safer battery systems and other metal-based electrode materials that are abundant on Earth to create a better energy storage system.^[4] Aqueous system zinc (Zn)-ion batteries have become a strong contender for future electric energy storage applications due to their cost effectiveness, environmental friendliness, safety and competitive energy density.^[5]

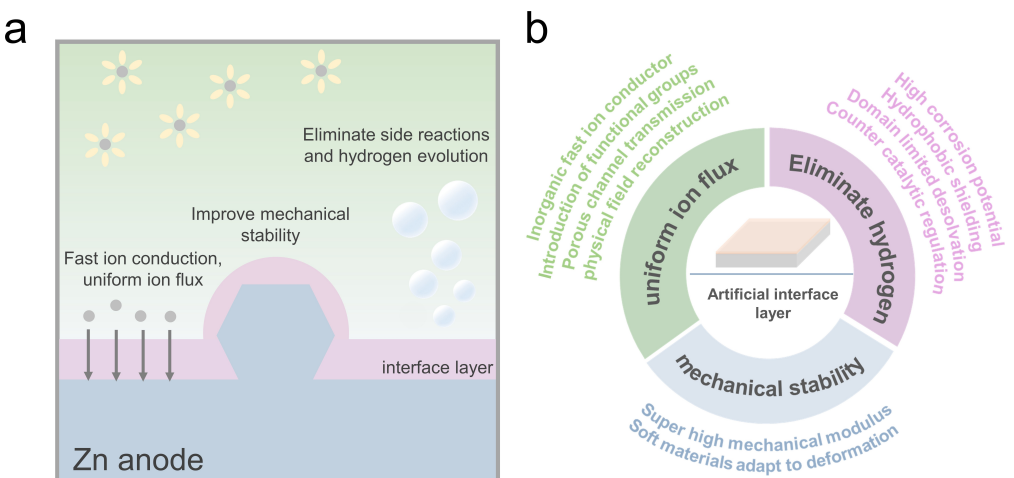
The Zn anode in aqueous system Zn-ion battery has a high theoretical mass capacity density of 820 mAh g^{-1} and volume capacity density of 5855 mAh cm^{-3} .^[6] In addition, Zn metal has a high redox potential (0.76 V vs. H⁺/H) in aqueous solution, which is suitable for Zn-air, Zn–Ni, Zn–MnO₂ and other Zn-based battery systems, showing a great application potential.^[7] Despite the potential of Zn as a anode, Zn has a distorted hexagonal dense arrangement, with each adjacent atom forming a hexagon coordination. The surface energy of each crystal surface of Zn varies greatly. Under the applied electric field, Zn shows a strong tendency to grow along the ab surface and deposit as hexagonal plates.^[8] This preferential growth of Zn in repeated cycles inevitably leads to the formation of irregular Zn dendrites.^[9] Because Zn has high mechanical properties, its Young's modulus is much higher than that of

lithium and sodium, which means that Zn dendrites, once formed on a large scale, can easily penetrate the diaphragm and grow.^[10] In addition, the high proton activity in the weak acidic electrolyte provides a stronger thermodynamic tendency for the hydrogen evolution reaction on the Zn surface, and the hydrogen evolution and corrosion problems become more serious.^[11] Hydrogen evolution and other side reactions compete with the Zn electrodeposition reaction, leading to continuous consumption of Zn metal and electrolyte solvents, resulting in low coulombic efficiency and swelling of the battery pack.^[12] Dendrites formation, corrosion and hydrogen evolution of Zn anode, low plating/stripping coulombic efficiency and poor cycle stability are still obstacles to the use of zinc anode (Scheme 1a).^[4b,13]

The above problems of the Zn anode are closely related to the plating and stripping behavior of Zn at the electrode interface.^[14] The electrode interface is the center of various physical and chemical interactions, and is the place where ion transport, electrochemical reactions and mechanical changes are coupled.^[15] Therefore, it is very important to optimize the interface design of Zn anode, and the construction of an effective artificial interface layer (AIL) is one of the most direct and effective methods to protect Zn anode, which is helpful to improve the cycle life of Zn anode.^[16] In recent years, both academia and industry have made a lot of efforts to solve these problems. With the continuous technological breakthroughs in the field of nanomaterials, researchers have investigated many effective AILs to inhibit the growth of Zn dendrites.^[17] However, there is a lack of effective design principles to guide the design and construction of higher performance interface layers in the future, so it is necessary to effectively summarize the progress of artificial interface layers to establish reliable design principles.

Based on the understanding of the interface problem of Zn anode, the design principles of the interface layer are mainly focused on three aspects: 1) uniform and fast transport of ions; 2) inhibition of corrosion and hydrogen evolution reaction; 3) mechanical stability (Scheme 1b). All of these factors are critical, and their effects should be considered in the design. In order to enable researchers to have a deeper understanding of the interface of Zn anode, understand the role of the protective layer of Zn anode interface. In this review, we through to the latest research progress on the track, these principles are discussed in detail on the properties of interface layer. It is hoped that the theoretical principles provided can better guide

[a] Z. Guo, Prof. L. Fan, Prof. N. Zhang
School of Chemistry and Chemical Engineering
Harbin Institute of Technology
Harbin 150001, China
E-mail: fanlsh@hit.edu.cn
znmww@163.com
[b] L. Wu, B. Li
Jiangsu Zhitai New Energy Technology Co., Ltd.
Taizhou, 225300, China



Scheme 1. a) Problems of Zn anode and required functions of interface layer. b) Design principles of the artificial interface layer.

the design of excellent interface layer to stabilize the Zn anode interface, so as to achieve the purpose of practical application.

2. Principle I: Fast Ion Conduction, Uniform Ion Flux

Zn^{2+} diffuses slowly in AILs due to the kinetics of the desolvation process at the electrode/electrolyte interface. This is due to the strong Coulombic interaction between the solvated ion and its surrounding solvent. The speed of ion transport in the interfacial layer is the key to uniform deposition, which affects the overall performance of Zn metal anode.^[18] Some studies have shown that dendrite growth is inhibited when electrolytes with higher ionic conductivity and higher migration number are used.^[15a,19] Uneven deposition is the beginning of a vicious cycle and dendrites growth. In order

to solve the Zn problem fundamentally, it is very important to adjust the spatial uniformity of the artificial interface layer. Therefore, in the design of the interface layer, it is very desirable to obtain a protective layer with uniform Zn^{2+} flux, faster transport speed and higher migration number.

2.1. Transport of inorganic fast ion conductors

Ionic conductors with high Zn^{2+} conductivity are ideal materials for the interface layer of zinc anode. Solid electrolyte interfacial film (SEI) exists on organic electrolyte and anode interface of battery with low operating potential.^[20] The organic solvent in the electrolyte can be reduced by the anode, and its reduced products become part of the SEI. However, aqueous electrolyte can not do this, because solute salt and water are reduced products of hydrogen and corrosion products, it is impossible to become effective SEI components. Therefore, it is



Zhikun Guo received his master's degree from the School of Chemical Engineering and Chemistry, Harbin Institute of Technology in 2019. He is now studying for his doctorate at Harbin Institute of Technology. His main research interest is Zn anode in Zn ion batteries for aqueous systems.



Naiqing Zhang is a professor in Harbin Institute of Technology (Harbin, China) and the fellow of the Royal Society of Chemistry (FRSC). He received his Ph.D. degree from Harbin Institute of Technology. He is now the director of the Institute of Chemistry and Energy Materials (HIT). His research interests focus on energy storage and conversion materials, devices and system integration including fuel cells, lithium secondary power batteries, aqueous zinc ion batteries, etc.



Lishuang Fan received his Ph.D. degree in 2015 from Harbin Institute of Technology (Harbin, China). He is now working as an associate professor in Harbin Institute of Technology. He worked as a visiting scholar at Centre for Clean Energy Technology, Faculty of Science, University of Technology Sydney under the supervision of Prof. Guoxiu Wang. His current research interests are mainly focused on lithium-sulfur battery, lithium-ion battery, sodium-ion battery and Zn-ion battery.

necessary to consider how to artificially construct an AIL, or convert the solute salts or other additives of the electrolyte into a part of the AIL in aqueous batteries.

SEI will be generated *in situ* in the electrolyte due to the strong activity of Li metal. A large number of studies have found that LiF in SEI has high ionic conductivity and is the main component of SEI ion transport.^[21] Inspired by this, some research efforts have been devoted to introducing *in situ* fluorinated interfaces on the Zn anode surface. Li et al. designed a 3D ZnF₂ interfacial protective layer on the zinc surface through a simple growth method, which redistributed the Zn²⁺ flux by reducing the desolvation activation energy and enhanced the electrochemical reversibility of the zinc metal.^[22] Zhi et al. also constructed ZnF₂ solid ion conductor to isolate Zn metal from electrolyte and achieve stable and convenient zinc deposition kinetics (Figure 1a). They measured a Zn²⁺ transfer number of 0.65 and an ionic conductivity of 80.2 mS cm⁻¹ for the ZnF₂.^[23] Wang et al. reported that Me₃EtNOTF as an electrolyte additive can form a fluoridation hydrophobic interface, inhibit the side reaction of hydrogen evolution and conduct Zn²⁺ at the same time. Thus, the Coulombic efficiency of Zn plating/stripping is increased from 87.6% to 99.9%.^[24] Recently, Han found that ZnF₂ can allow Zn²⁺ insertion and provide diffusion channels for Zn²⁺ transport to and from the Zn anode through a gap diffusion mechanism that is different from the vacancy mechanism, as shown in Figure 1(b).^[25] In addition, a small amount of DMSO to the Zn(TFSI)₂ electrolyte was found to significantly increase the proportion of TFSI⁻ anion in the Zn²⁺ primary solvated sheath.

In this way, TFSI⁻ anion can be reduced well before zinc deposition, thus forming ZnF₂-rich interfacial phase *in situ*.^[26] Kim et al. diffused Zn into the MgF₂ layer to form a gradient MgF₂ interfacial phase. The interfacial polarization (Maxwell-Wagner effect) between the Zn-doped MgF₂ region and the MgF₂ layer results in rapid Zn transfer kinetics.^[27]

The introduction of other appropriate elements doped into the Zn lattice to form an interfacial layer can change the charge distribution on the zinc surface, thereby driving faster Zn²⁺ diffusion during cycling. Guo's team skillfully prepared the dense ZnS layer *in situ* through the vapor-solid reaction. The dense interface layer not only can effectively inhibit the corrosion, but also has a high zinc ion migration number (Figure 1d).^[28] Similarly, Sun et al. constructed an *in situ* grown ZnSe overlay on one side of a commercial zinc foil by chemical vapor deposition to achieve efficient interface manipulation, as shown in Figure 1(c). The initially disordered Zn processes are transformed into ZnSe nanoparticles after selenization to form an ultrathin ZnSe layer, which binds uniformly to the Zn metal to form a heterostructured ZnSe@Zn. The ZnSe thus derived plays a role in guiding the growth of Zn along the (002) crystal plane.^[29] In addition, Zn-phosphorus solid solution alloy (ZnP) was prepared on Zn foil by efficient electrodeposition method to achieve fast charging and high area capacity.^[30]

Other inorganic oxides also have high ionic conductivity, adding a layer of ionic conductor at the electrode interface will have a good effect on extending the battery life. By coating the Zn with a TiO₂ protective layer with a highly exposed (001) surface, Wang et al. can prepare a high performance zinc anode

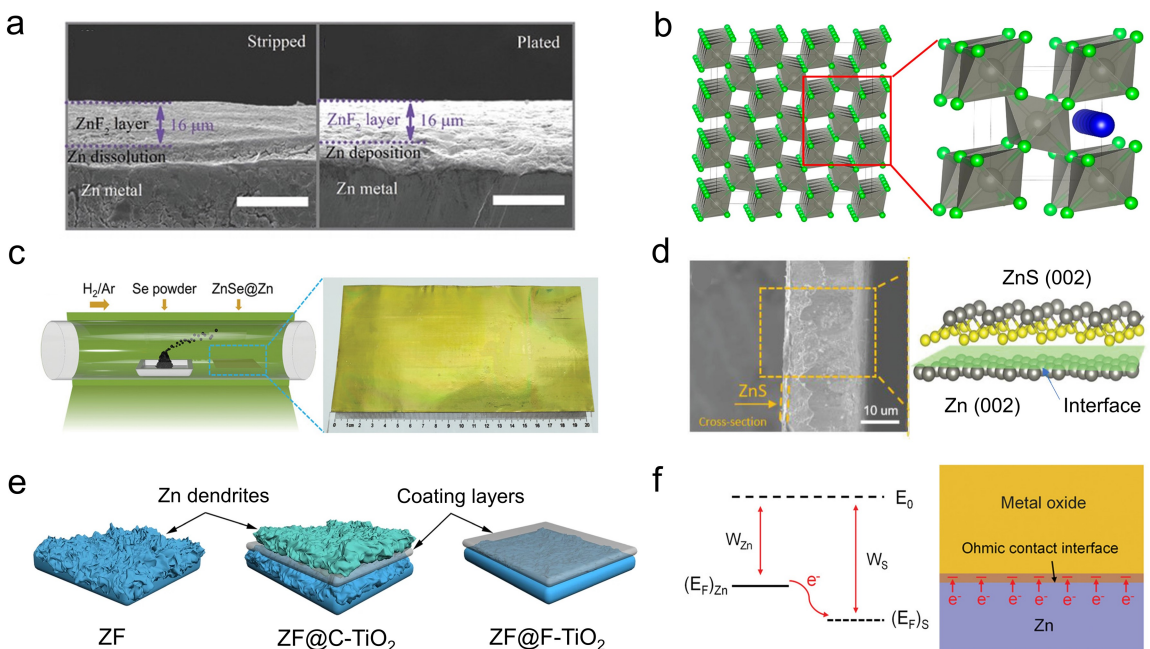


Figure 1. a) Cross-sectional SEM images of Zn stripping (left) and Zn plating (right) on Zn@ZnF₂. Reproduced with permission from Ref. [23]. Copyright (2021) Wiley-VCH. b) Schematic diagram of the mechanism of Zn²⁺ diffusion in the ZnF₂ gap. Reproduced with permission from Ref. [25]. Copyright (2021) American Chemical Society. c) In situ construction of ZnSe coating on zinc foil by chemical vapor deposition. Reproduced with permission from Ref. [29]. Copyright (2021) Wiley-VCH. d) Dense ZnS prepared on zinc surface in situ. Reproduced with permission from Ref. [28]. Copyright (2020) Wiley-VCH. e) Schematic diagram of Zinc deposition on TiO₂ layer with exposed different crystal planes. Reproduced with permission from Ref. [31]. Copyright (2020) Springer Nature. f) Ohmic contact model of zinc-metal oxide interface. Reproduced with permission from Ref. [35]. Copyright (2021) Wiley-VCH.

without external dendrite growth is shown in Figure 1(e). Benefiting from the specific crystal orientation of TiO_2 and the repulsion of Zn adsorption, Zn^{2+} are enriched on the surface of the anode under the action of electric field. Increased interfacial Zn^{2+} concentration can induce homogeneous nucleation and further guide zinc lateral growth.^[31] Yi et al. used a ZrO_2 coating to promote uniform plating of the Zn. Due to its high permittivity ($\epsilon \approx 25$), low electrical conductivity, and good chemical stability, ZrO_2 experiences favorable Maxwell-Wagner polarization (referred to as "space-charge polarization")^[32] during electrochemical processes. This polarization can provide a controlled nucleation site for Zn^{2+} and facilitate rapid ionic dynamics.^[33] A similar type of polarization can be produced by Sc_2O_3 coatings.^[34] Liu et al. demonstrated a universal Ohmic contact interface model, which can effectively improve the reversibility of zinc plating/stripping (Figure 1f). As a proof of concept, the CeO_2 layer improves the diffusion kinetics of Zn^{2+} and reduces the nucleation barrier of Zn.^[35] In addition, some inorganic materials (such as $\text{NaTi}_2(\text{PO}_4)_3$,^[36] MMT,^[37] etc.) also have the characteristics of fast ion conductors, which will be introduced in the following content.

2.2. Introducing functional groups

Anion groups in aqueous electrolyte are the main components of by-products. Some negatively charged groups are used to screen and repel anions to prevent their migration to the electrode surface, and the migration number of Zn ions can also be increased. Figure 2(a) shows that He et al. fabricated an AIL with an anion concentration gradient (ACG) for achieving ultra-high ionic conductance through chemical reactions of sulfonic acid polymers and Zn. The driving effect of sulfonate concentration gradient promotes the transport of Zn^{2+} and inhibits the diffusion of anion in the interfacial layer.^[38] Wang et al. introduced a negative charge layer combined with a metal-organic skeleton containing functional groups (UIO-66-SO₃H) and flexible sulfonated polyether ether ketone (SPEEK) binder on the Zn anode. Since UIO-66 modified by SO₃⁻ can repel the anion SO₄²⁻, the solvation structure of Zn²⁺ is manipulated.^[39] Zhang et al. designed and prepared a layer with SO₄²⁻ trapping capability (Zn@SR) to improve zinc anode cycle stability. SR molecules with a large number of -NH groups can "trap" SO₄²⁻ in the electrolyte through -NH...O hydrogen bonds. The resulting negatively charged SR-SO₄²⁻ layer can attract Zn²⁺ in the electrolyte through electrostatic interaction and accelerate the migration of Zn²⁺ to the negative electrode (Figure 2b).^[40] In addition, they designed a layered double oxide coating (LDO) derived from Zinc-aluminum hydroxide. LDO captures anion by electrostatic attraction in ZnSO₄ electrolyte, which reduces the concentration gradient of Zn²⁺ and avoids the savage growth of dendrites.^[41] By introducing a polyanionic hydrogel film as a protective layer (Zn-SHn) on the zinc anode with the help of a saline coupling agent. Polyanion hydrogel films containing negatively charged -SO₃⁻ can effectively promote Zn²⁺ desorption and repulsion of anions, and maintain uniform ion fluxes (Figure 2c).^[42] These

anion shielding strategies open a new way for the design of stable zinc negative interface structures.

Some organic polar functional groups can show strong chemical interaction with Zn²⁺, and these functional groups can be used to regulate the ion transport path and speed in the AIL. For example, the β -PVDF film can be used as a channel and buffer layer for guided ion transport at the zinc anode interface. The β -PVDF coating is composed of stacked F atoms aligned in the same direction, and Zn²⁺ is rapidly permeated into the coating by strong interaction with the electronegative C-F functional group as shown in Figure 2(d).^[43] Liu et al. constructed an ion-adhering cellulose acetate (CA) coating on zinc anodes. Due to the complexation between polar ester group (C-O) and Zn²⁺, the CA coating enhances the Zn philicity of zinc anode, reduces the interfacial resistance, and makes Zn²⁺ diffuse rapidly in aqueous electrolyte (Figure 2e).^[44] Yan et al. prepared a cyano-rich AIL for zinc anode by coating polyacrylonitrile (PAN) and soluble zinc salt to achieve rapid desolvation kinetics. Because PAN is rich in cyano groups, it can provide enough coordination sites to attract hydrated solvation sheaths, thus reducing the desolvation activation energy and improving the kinetics of zinc ion deposition (Figure 2f).^[45]

2.3. Fast transmission through porous channels

Porous channels can provide rich ion transport paths, and selective modification of the channels can also play a role in desolvation. Kang et al. developed a simple and economical nanoporous coating strategy to improve the stripping/plating stability of zinc metal anodes (Figure 3a). The nano-CaCO₃ porous layer is confined to the surface region of the zinc foil to guide a uniform Zn²⁺ flux.^[46] Zhu et al. developed a fast ion conductor NaTi₂(PO₄)₃ (NTP) porous nanoparticle as AIL to induce homogeneous deposition of Zn²⁺. The interstitial lattice migration barrier of NTP is small. It is confirmed that Zn²⁺ can be transported in the constructed NTP "ion fence" (Figure 3b).^[36] A Prussian blue analogue (CuHCF) with a 3D open structure and polar rich group (CN), was coated on zinc foil as AIL. The ion conductivity of CuHCF AIL is 7.6 mS cm⁻¹, and the Zn²⁺ transfer number is 0.74.^[47]

Similar to ion screening through multiple channels to accelerate ion diffusion are two-dimensional materials. For example, the abundant ion channels in the Mg-Al LDH can efficiently redistribute Zn²⁺ fluxes near the interphase at a fundamental level, much like a dam spillway dredging flood, leading to ultra-stable zinc plating/stripping behavior below the AIL. In addition, montmorillonite (MMT) materials are successively developed as AIL to inhibit the growth of Zn dendrites. The lamellar structure in MMT acts as a highway for cation transport, and the migration of Zn²⁺ into the interlayers driven by the electric field ensures a high Zn²⁺ migration number ($t_+ \approx 0.82$) and ionic conductivity ($\sigma \approx 3.93 \text{ mS cm}^{-1}$).^[37] Vermiculite provides two-dimensional fluid channels similar to molecular sieve pores, which can effectively regulate ion migration, as shown in Figure 3(c). Due to the "ion acceleration effect" of the VRM nanochannel, the ion concentration gradient

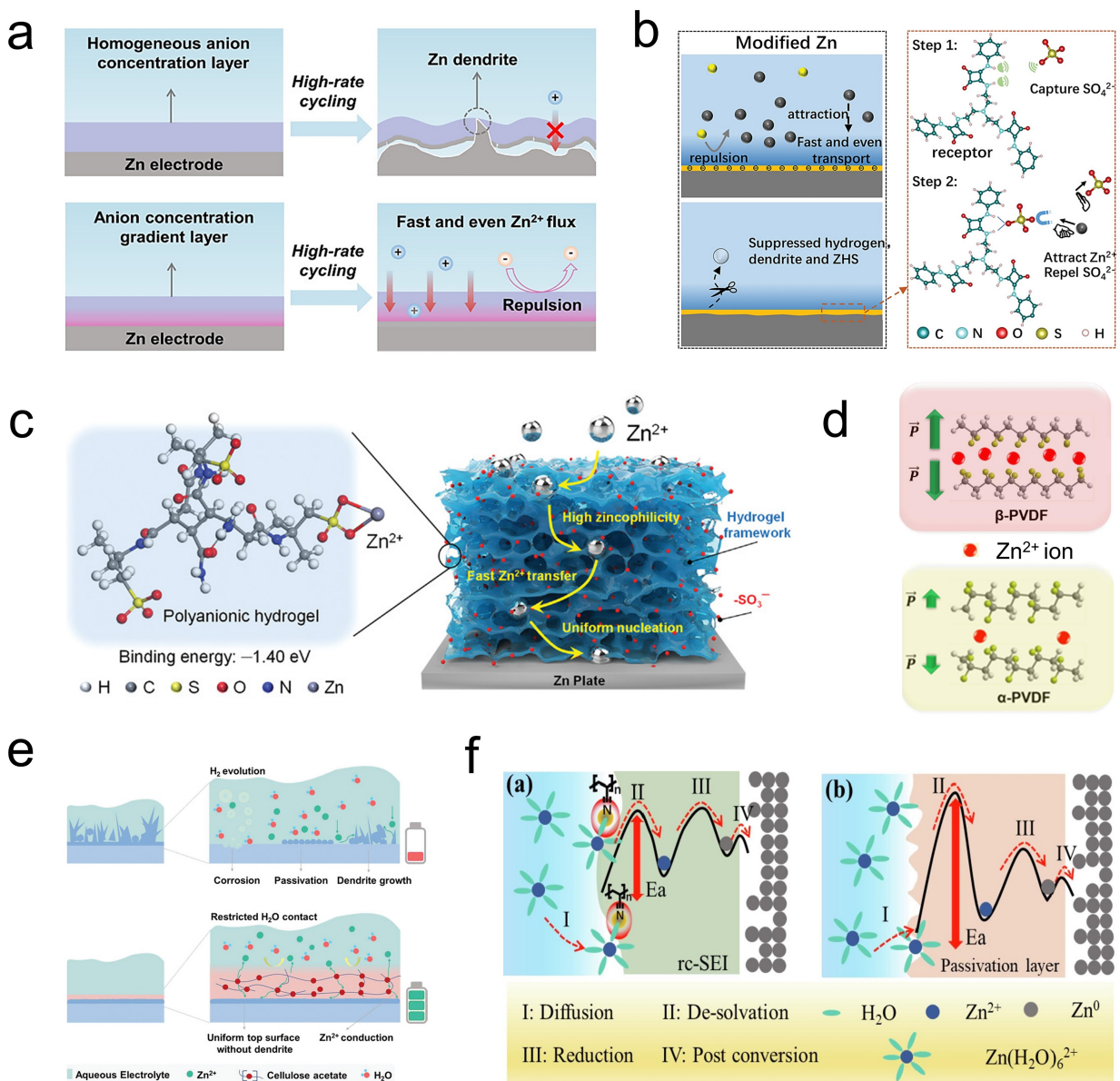


Figure 2. a) AIL with anion concentration gradient achieves ultra-high ionic conductance. Reproduced with permission from Ref. [38]. Copyright (2022) American Chemical Society. b) The –NH group “captures” SO₄²⁻ through the N–O bond. Reproduced with permission from Ref. [40]. Copyright (2022) Wiley-VCH. c) Effect of negatively charged SO₃⁻ polyanion hydrogel film. Reproduced with permission from Ref. [42]. Copyright (2022) Wiley-VCH. d) Zn²⁺ migration in β-PVDF. Reproduced with permission from Ref. [43]. Copyright (2021) Elsevier. e) Mechanism of ionic adhesive cellulose acetate coating. Reproduced with permission from Ref. [44]. Copyright (2022) Wiley-VCH. f) The –CN group of PAN attracts the solvation shell to reduce the activation energy of desolvation. Reproduced with permission from Ref. [45]. Copyright (2022) Elsevier.

at the anode/electrolyte interface is reduced.^[48] Zeolite molecular sieve has been studied for many years and is widely used because of its uniform microporous structure. Zhou et al. made thin films of molecular sieve, used pore structure to adjust the solvation shell of hydrated ions.^[49] Inspired by the concept of “water in salt”, the zinc anode coated with a molecular sieve with ordered mesoporous channels can induce the formation of local high concentration electrolyte at the interface (Figure 3d).^[50]

Metal organic frameworks (MOFs) are considered as promising interfacial layer for zinc anodes due to their porous structure and the insulating properties of electron blocking.^[51]

Pan et al. proposed an AIL consisting of a MOF to improve the wetting effect of aqueous electrolyte on Zn anode. Hydrophilic MOF nanoparticles can achieve a good wetting effect and adjust the electrolyte flux on Zn anode (Figure 4a).^[52] The porous ZIF-8 grown in situ can be used as a screening protective layer for Zn²⁺. The ordered nanochannels can divide the space above the anode into small constraints, and the Zn²⁺ flux in each constraint nanochannel is relatively uniform (Figure 4b).^[53] Figure 4(c) shows that Wang et al. separated the aqueous electrolyte from the zinc anode by coating the anode with a thin MOF layer and filling the pores of the MOF with a hydrophobic Zn(TFSI)₂-TFEP organic electrolyte incompatible

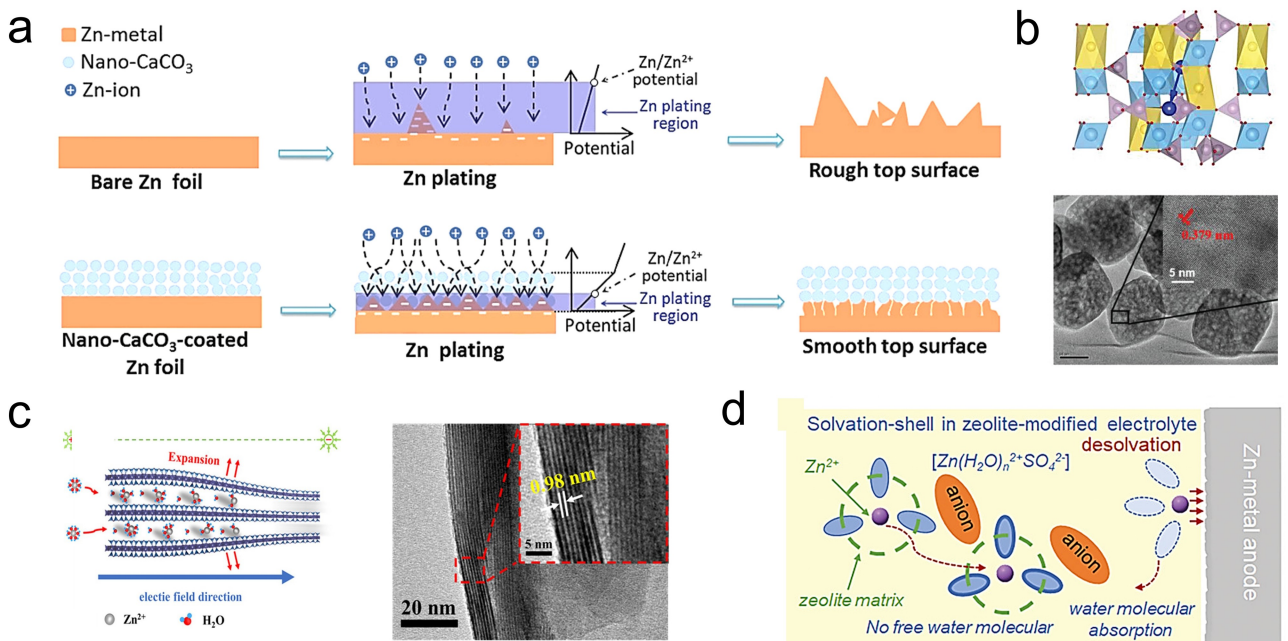


Figure 3. a) Schematic illustrations of morphology evolution for bare and nano-CaCO₃ coated Zn during Zn stripping/plating cycling. Reproduced with permission from Ref. [46]. Copyright (2018) Wiley-VCH. b) Schematic pictures of Zn ion migration pathways for NaTi₂(PO₄)₃ (TOP). TEM image of NaTi₂(PO₄)₃ nanoparticle. Reproduced with permission from Ref. [36]. Copyright (2020) Wiley-VCH. c) Schematic diagram of Zn²⁺ transport in the VRM nanochannels, and TEM images of VRM layer. Reproduced with permission from Ref. [48]. Copyright (2022) Elsevier. d) In the zeolite-modified electrolyte, the hydrated water molecule is largely reduced, and the solvation sheath is highly coordinated. Reproduced with permission from Ref. [49]. Copyright (2021) Wiley-VCH.

with the H₂O. Zn(TFSI)₂-TEEP@MOF forms a ZnF₂-Zn₃(PO₄)₂ AIL, which prevents the decomposition of Zn dendrites and water, and can achieve 99.9% reversible plating/stripping coulombic efficiency.^[54]

Covalent organic frameworks material is a kind of porous crystalline organic material. This kind of material has the advantages of strong covalent force between skeletons, low weight density, orderly channels and customizable functional groups, so it is widely used in the field of energy storage. Sodam et al. first proposed a single-ion conducting COF as a Zn²⁺ battery electrolyte (Figure 4d). The fixed and delocalized sulfonate of TpPa-SO₃Zn_{0.5} in the directional pore enables single transport of Zn²⁺.^[55] Grzybowski et al. developed scalable deposition of COF precursor solutions over large areas and arbitrary substrates by a simple dip coating technique. They achieved self-assembly of large-area, flexible, nanoporous, and ultrathin COF films directly on zinc anodes, as shown in Figure 4(e).^[56] An important feature of COFs is the ability to tailor functional groups to needs. Guo et al. developed a two-dimensional FCOF containing fluorine as an AIL to protect the Zn anode (Figure 4f and g). FCOF nanochannels containing F can provide rapid Zn²⁺ transport channels and uniformly distributed nucleation sites. The strong interaction between fluorine (F) and Zn reduces the surface energy of Zn(002) crystal surface, which makes the (002) crystal surface grow preferentially during electrodeposition.^[57]

2.4. Interfacial electric field reconstruction

The electric field and concentration field in the AIL will affect the fast ion transport. It is well known that ferroelectric materials will generate polarization and form internal electric field in the presence of external electric field, which will accelerate ion transport dynamically.^[58] BTO is a typical ferroelectric material^[59] and Zhang et al. used BTO to construct AIL, which can guide the ordered migration of Zn²⁺ through uniform ion pathways and directional dipoles provided by the BTO layer (Figure 5a).^[60] However, the self-generated electrostatic field of the cell is weak and the polarization of the ferroelectric layer along the vertical direction of the anode is limited. Xin et al. used a high-voltage corona polarized pre-polarized ferroelectric layer to replace the original ferroelectric layer, so that the piezoelectric properties of the layer along the polarization direction can be fixed and improved to the maximum extent (Figure 5b).^[61] In addition, ferroelectric polymers have attracted extensive attention due to their advantages of low processing temperature and good flexibility. PVDF-TrFE can act as AIL to provide an internal electrostatic field between PVDF-TrFE and zinc to accelerate ion transport because the dipole orientation of the molecule can be changed during the DC polarization process (Figure 5c and d).^[62] In addition, amorphous Si₃N₄ nanoparticles possess abundant dangling bonds (N≡Si, Si₂≡N, etc.), which are capable of confining large space charges. Under an external electric field, the dipole moment can be aligned with a specific direction, thus promoting the homogenization of Zn electrodeposition, as shown in Figure 5(e).^[63] The uniform distribution of the

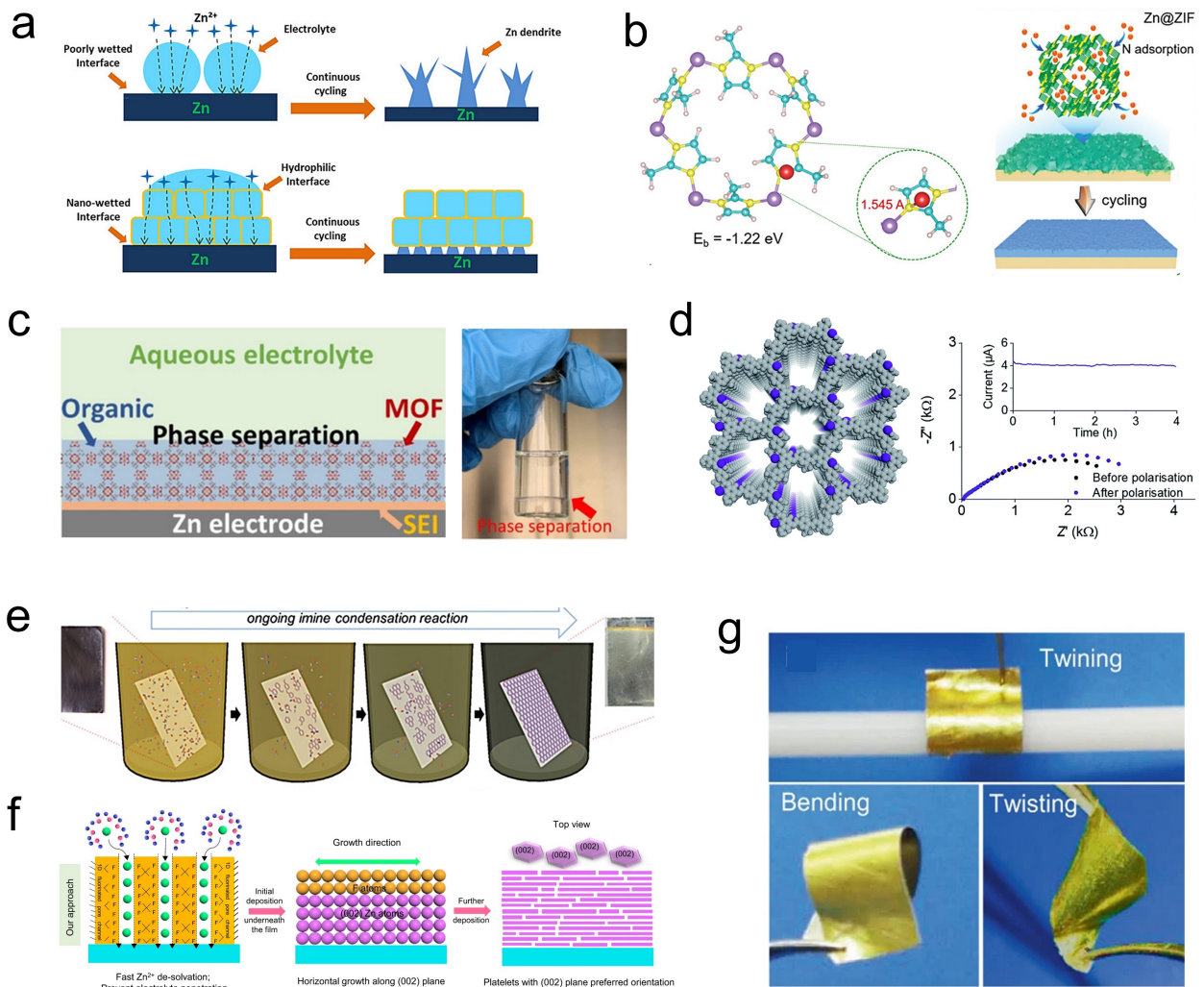


Figure 4. a) Hydrophilic MOF can improve the wetting effect of electrolyte on Zn anode. Reproduced with permission from Ref. [52]. Copyright (2019) American Chemical Society. b) ZIF-8 acts as a sieving AIL for Zn²⁺ to regulate Zn plating behavior. Reproduced with permission from Ref. [53]. Copyright (2020) Wiley-VCH. c) The MOF well was filled with hydrophobic Zn(TFSI)₂-TFEP organic electrolyte and SEI was formed. Reproduced with permission from Ref. [54]. Copyright (2020) Wiley-VCH. d) TpPa-SO₃Zn_{0.5} COF enables single ion transport of Zn²⁺. Reproduced with permission from Ref. [55]. Copyright (2020) Royal Society of Chemistry. e) The dip coating technique self-assembles large area COF film directly on zinc anode. Reproduced with permission from Ref. [56]. Copyright (2021) Wiley-VCH. f) The strong interaction between F and Zn²⁺ in FCOF makes the (002) crystal surface grow preferentially during plating. g) The FCOF layer is tightly bound to Zn. Reproduced with permission from Ref. [57]. Copyright (2021) Springer Nature.

concentration field in the interfacial layer also has an important effect on the uniform deposition of ions. Zhi et al. introduced hydrogen atoms into the benzene ring of graphite dialkyne (GDY) and modified it to produce hydrogen substituting HsGDY with semiconducting properties. Figure 5(f) shows that HsGDY uses its interconnected sub-angstrom ion tunnels to spatially force Zn²⁺ away from the direction of the electric field, and then forms a relatively uniform concentration field along the interface.^[64]

An uneven surface will make the electric field distribution uneven, easy to produce dendrite growth hotspots. It is also an effective method of uniform ion flux to adjust the interfacial electric field and current distribution during zinc deposition by using conductive materials. Li et al. constructed inexpensive porous carbon layers on the surface of zinc foils, which promoted uniform current distribution and zinc deposition,

thus improving the kinetics of zinc dendrites.^[65] The use of ZIF-8 derived carbon nanoparticles as hosts for the electrodeposition of Zn has been reported in the literature (Figure 5g).^[66] In addition, the introduction of some defects in the carbon layer will increase the affinity to zinc. He et al. used three-dimensional porous nitrogen doped carbon on the zinc anode (3D-NC@Zn) in Figure 5(h). And the N and O functional groups of the three-dimensional carbon network provided good Zn adsorption sites, so as to realize the stable and rapid deposition of Zn.^[67] However, it should be noted that many carbonaceous materials are rich in defects, such as vacancies and doped heteroatoms, which may act as active sites for catalytic hydrolysis, and impair the electrochemical performance and calendar life of anode.

Compared with porous carbon, conductive materials with high flexibility and large specific surface area have stronger

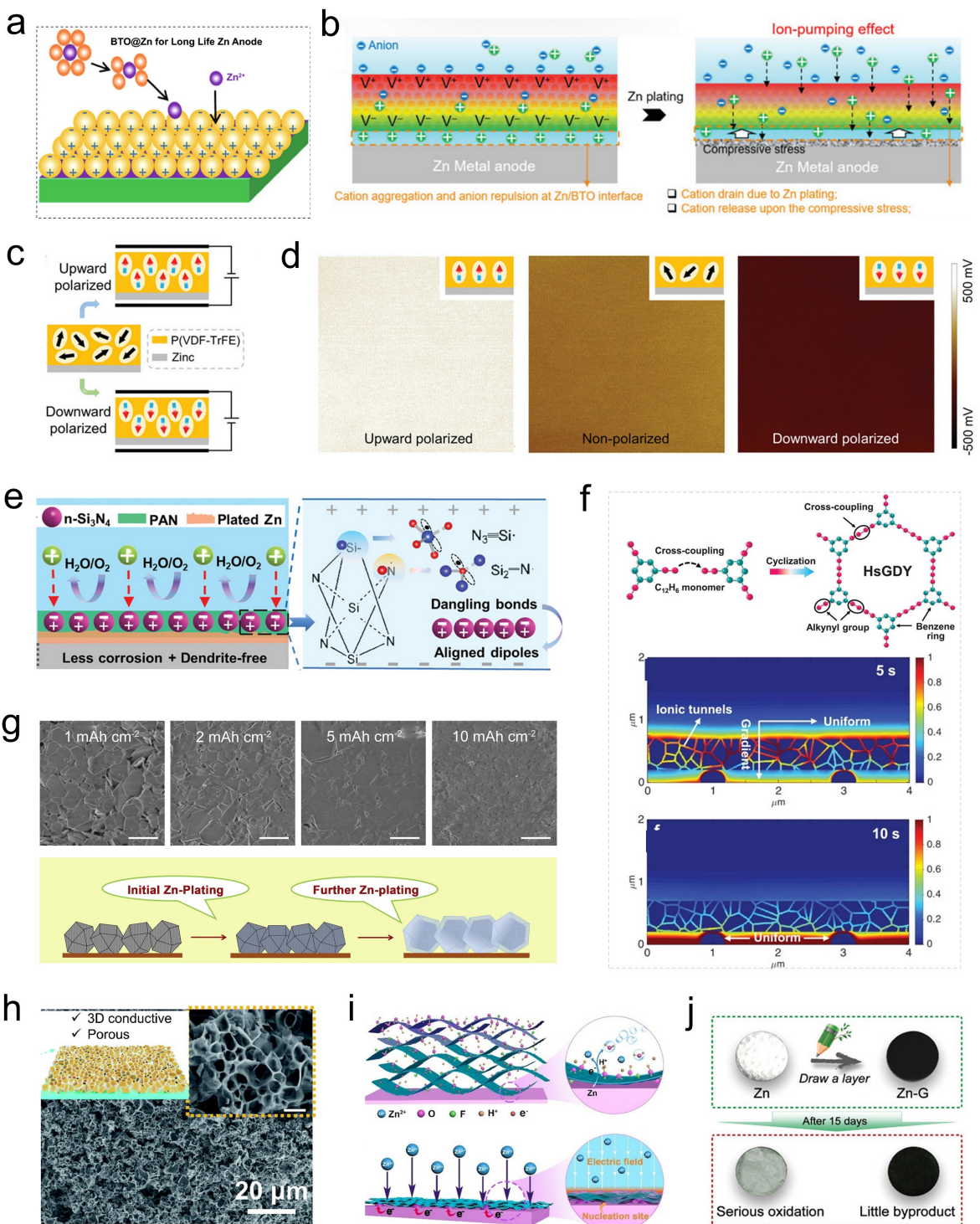


Figure 5. a) The polarization induced by BTO layer can guide the migration of Zn^{2+} . Reproduced with permission from Ref. [60]. Copyright (2021) Springer Nature. b) The performance of BTO is improved by using high voltage corona prepolarization. Reproduced with permission from Ref. [61]. Copyright (2021) Wiley-VCH. c) Schematics showing the polarization process of PVDF-TrFE coating. d) Kelvin probe force microscopy images of PVDF-TrFE-coated zinc anodes with varying dipole directions. Reproduced with permission from Ref. [62]. Copyright (2022) Wiley-VCH. e) Schematic illustration of Zn plating/stripping behavior with coating (left). The amorphous Si_3N_4 exhibit novel dielectric behavior (right). Reproduced with permission from Ref. [63]. Copyright (2021) Wiley-VCH. f) HsGDY uses subangstrom ion tunnels to form a uniform concentration field of Zn^{2+} in space along the interface. Reproduced with permission from Ref. [64]. Copyright (2020) Wiley-VCH. g) ZIF-8 derived carbon nanoparticles were used as hosts for Zn electrodeposition. Reproduced with permission from Ref. [66]. Copyright (2019) Elsevier. h) Three dimensional porous nitrogen doped carbon layer. Reproduced with permission from Ref. [67]. Copyright (2022) Royal Society of Chemistry. i) Charge redistribution effect in self-assembled MXene layers. Reproduced with permission from Ref. [70]. Copyright (2021) Wiley-VCH. j) The pencil drawing method was used to produce an inexpensive zinc anode conductive interfacial layer. Reproduced with permission from Ref. [71]. Copyright (2021) Wiley-VCH.

interfacial electric field regulation ability. Researchers have fabricated highly flexible and electrically conductive carbon nanotube scaffolds by dipping and drying. The porous skeleton of the CNT scaffold can mechanically regulate the deposition sites on the surface of the zinc electrode and maintain a stable electric field, thus delaying the formation of dendrites.^[68] Xie constructed a protective layer of nitrogen-doped graphene (NGO) on zinc foil using a simple method. The conductive NGO artificial protective layer helps to balance the interfacial electric field and inhibit the growth of zinc dendrite tips.^[69] Niu et al. first assembled a homogeneous conducting MXene layer on the surface of a Zn anode using a self-assembly strategy. The charge redistribution effect of MXene layer makes the anode have the advantages of low nucleation barrier and uniform electric field distribution, so that the zinc deposition is uniform (Figure 5i).^[70] Recently, a very simple penciling method has been used to produce inexpensive conductive interfacial layers for zinc anodes (Figure 5).^[71] The graphite layer has a uniform electric field distribution, which can be used not only as a soft buffer layer for Zn^{2+} migration but also as a porous nuclear inducer for deposition. More importantly, this approach solves the problem of high cost such as graphene and MXene.

Although the introduction of electron uniform layer with high electron conductivity helps to avoid the charge accumulation during the cycling process. However, it should be noted that when the interfacial layer is conductive, Zn^{2+} prefer to obtain electron reduction on the surface of the interface layer. At the same time, if a strong hydrogen evolution reaction occurs on the negative electrode surface, whether the stability of the interface layer can be maintained is a problem.

3. Principle II: Eliminate Side Reactions and Hydrogen Evolution

The difficulty of aqueous battery application is that its lifetime and energy density are limited by the narrow electrochemical stability window of aqueous electrolyte. Thermodynamically, this electrochemical window is only 1.23 V. The corrosion

reaction of anodes in aqueous zinc-ion batteries occurs spontaneously, continuously consuming active electrodes and electrolytes.^[72] For example, after immersion in 3.0 M $ZnSO_4$ solution, the zinc anode was severely corroded and covered with a loose sheet of irreversible $Zn_4(OH)_6SO_4 \cdot 5H_2O$ byproducts, leading to passivation of the zinc anode and loss of active electrode (Figure 7a).^[73] It is worth noting that in the weak acidic electrolyte, the hydrogen evolution reaction occurs at the same time as the electrochemical corrosion of Zn. When the electron energy level (work function) corresponding to the anode reaction potential of the battery is higher than the lowest unoccupied molecular orbital (LUMO) of water molecules, hydrogen ions in the electrolyte will be reduced to form hydrogen molecules (Figure 6a^[74] and b). The continuous corrosion and hydrogen evolution reaction lead to the continuous decomposition of electrolyte and rapid consumption of active zinc, the increase of electrode interface impedance, low coulombic efficiency (CE) and battery pack expansion.^[75] Therefore, another key purpose of interface protective layer design is to minimize the side reaction between zinc metal and liquid electrolyte, and reduce or even prevent the water molecules in the electrolyte from hydrogen evolution on the electrode surface to produce hydrogen.

3.1. Increase corrosion potential

In the corrosion reaction of zinc anode, the anode half reaction is the dissolution of metal to form by-products, and the cathode half reaction is the reduction of protons or water molecules to form hydrogen molecules. The hydrogen evolution reaction (HER) will proceed in two steps via the Volmer Heyrovsky mechanism, in which protons and water molecules, which are the sources of hydrogen in acidic and neutral solutions, respectively (Figure 7b).^[76] It should be noted that the water molecules involved in the corrosion reaction can be not only free water molecules, but also water molecules in the solvated sheath of cations and anions. The HER problem caused by corrosion can be solved from two perspectives: anode half-reaction and cathode half-reaction. For the anodic half reaction,

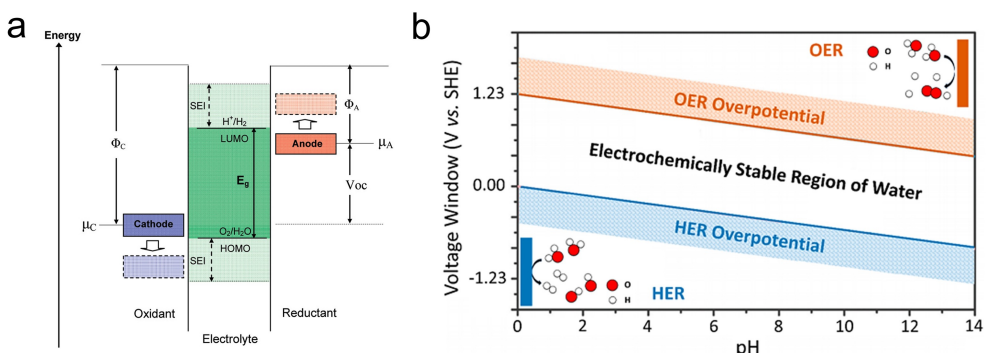


Figure 6. a) Schematic energy diagram of Zn anode and cathode in an aqueous electrolyte. Reproduced with permission from Ref. [74]. Copyright (2010) American Chemical Society. b) Pourbaix diagram of water in aqueous electrolytes. Reproduced with permission from Ref. [96]. Copyright (2021) American Chemical Society.

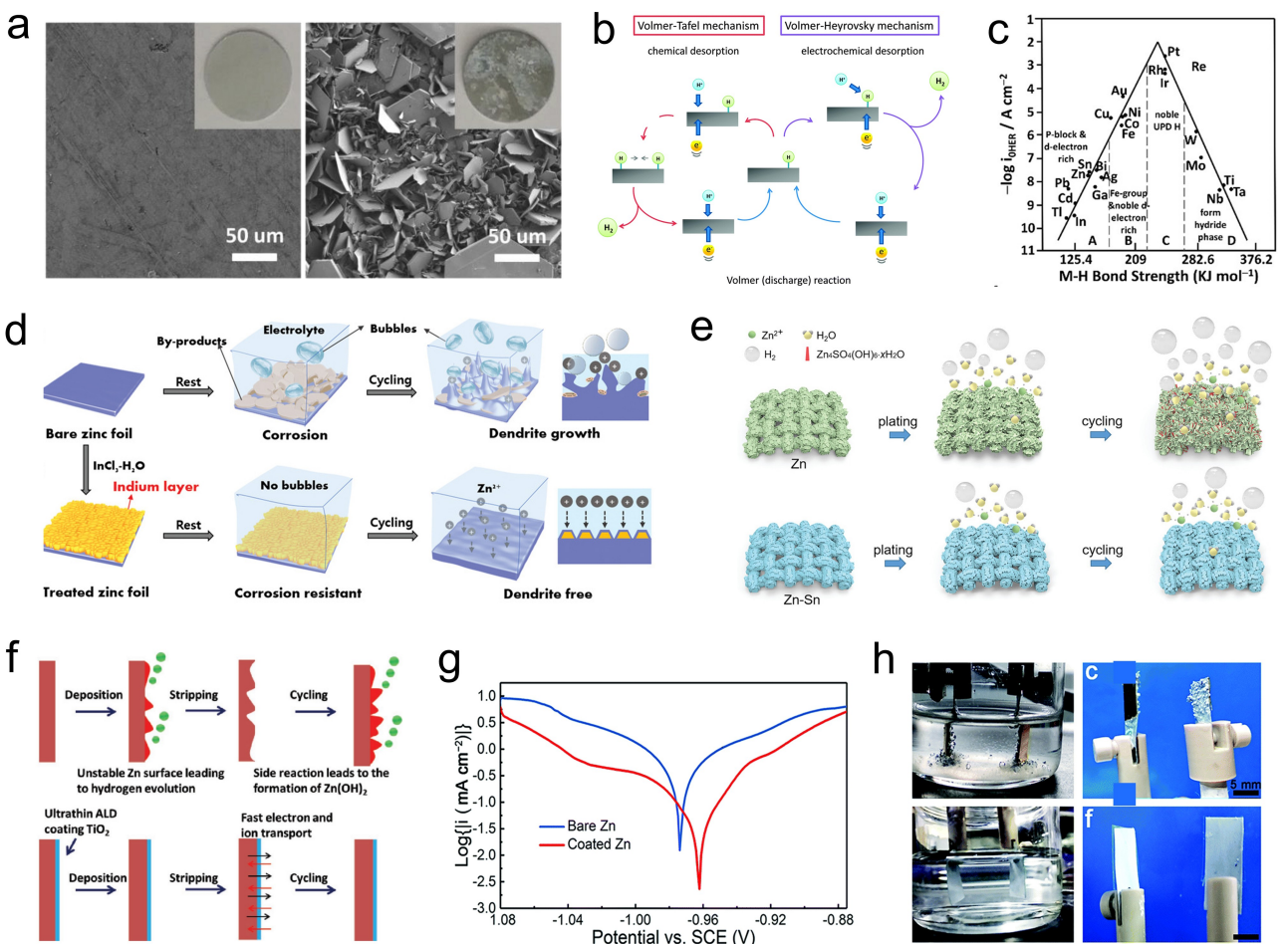


Figure 7. a) Top-view SEM images of (left) pristine Zn electrode and (right) Zn-30 day electrode. The insets showed the digital pictures of the corresponding electrodes. Reproduced with permission from Ref. [73]. Copyright (2020) Elsevier. b) The mechanism of hydrogen evolution on the surface of an electrode in acidic solutions. Reproduced with permission from Ref. [76]. Copyright (2014) Royal Society of Chemistry. c) Volcano plots for some metal HER catalysts under alkaline conditions. Reproduced with permission Ref. [77]. Copyright (2000) Elsevier. d) Schematics of the behavior of (top) bare Zn and (bottom) Zn|In anodes in an aqueous $ZnSO_4$ electrolyte. Reproduced with permission from Ref. [78]. Copyright (2020) Wiley-VCH. e) Sn alloying to inhibit hydrogen evolution of Zn metal anode. Reproduced with permission from Ref. [80]. Copyright (2022) Wiley-VCH. f) The decomposition of solvent (top) in aqueous electrolyte will accelerate the dehydration of Zn^{2+} , thus forming $Zn(OH)_2$ with poor conductivity. The thin layer of TiO_2 coating (bottom) eliminates the severe gas precipitation. Reproduced with permission from Ref. [82]. Copyright (2018) Wiley-VCH. g) Linear polarization curves showing the corrosion on bare Zn and coated Zn. h) Symmetrical zinc cell (top) exposed zinc plate and (bottom) coated zinc plate assembly side reaction during continuous zinc plating/stripping in a transparent tank. Reproduced with permission from Ref. [84]. Copyright (2019) Royal Society of Chemistry.

It is desirable to increase the oxidation potential of the metal, thereby reducing the overall electromotive force (voltage) of the corrosion reaction. For the cathodic half-reaction of corrosion reaction, the adsorption energy of H^* intermediate on the metal anode is the key factor affecting the hydrogen evolution rate.

In corrosion science, some metal (such as Pb, Bi, Hg, Ti, Sn, etc.) have naturally high corrosion and hydrogen evolution overpotential, which can form alloy interface layer to inhibit hydrogen evolution and corrosion, as shown in Figure 7(c).^[77] For example, the Cu/Zn composite anodic interface is prepared by growing a thin layer of Cu on the zinc metal surface in situ, and the deposited Cu and Zn form the alloy phase of Cu_5Zn_8 and $CuZn$. The corrosion potential of the CuZn alloy anode (E_{corr} , 0.964 V vs. SCE) was higher than that of the original Zn metal anode (0.976 V vs. SCE).^[73] A thin layer of indium (In) metal is introduced on the surface of Zn to inhibit corrosion.

The In layer modified at the Zn interface can act as both corrosion inhibitor and nucleating agent (Figure 7d).^[78] Similarly, Li et al. modified the Zn anode surface with In by ion exchange and found an ultra-compact and rock-like Zn deposition morphology without the formation of inert by-product.^[79] Recently, researchers have proposed an Sn alloying method to effectively inhibit hydrogen evolution and dendrite growth in Zn metal anodes (Figure 7e). Through in situ monitoring of hydrogen production in repeated electroplating/stripping tests, it was quantitatively proved that the hydrogen evolution of the alloy electrode with appropriate Sn amount was only half of that of the pure Zn electrode. Compared with pure zinc anode, Sn element increases the energy barrier of competitive hydrogen evolution in galvanizing process. Through the study of alloy electrodes with different Sn contents, it is found that the inhibition effect will be weakened with the increase of Sn content, so the more alloying elements

is not the better.^[80] The effect of alloy doping on HER performance of zinc anode was studied by Huang et al. The analysis of D-band center and Bader charge shows that Sn and Bi atoms acquire trivial electrons from adjacent Zn atoms, resulting in local distortion of the zinc anode. In addition, Sn and Bi doping both reduce the work function, which is conducive to the deposition of Zn atoms. Therefore, they suggested that alloy doping with less charge transfer, greater local distortion, and reduced zinc anodic work function may be beneficial to inhibit HER behavior.^[81]

Unfortunately, this layer conducts electricity at the interface, so the protection is temporary. Because zinc tends to deposit on top of conductive alloy coatings, corrosion remains a problem when zinc deposits are exposed to electrolytes. In addition, it can be solved by layer the zinc metal anode with some materials with low electrical conductivity but certain ionic conductivity. For example, some metal oxides have a good effect on inhibiting corrosion. Mai et al. applied a thin TiO₂ surface coating on zinc metal by ALD method. This ultrathin TiO₂ coating is a stable passivation layer of zinc metal, avoiding direct contact between zinc plate and electrolyte (Figure 7f). The corrosion potential decreased from -0.87 V vs. Ag/AgCl of bare zinc to -0.91 V of TiO₂@Zn, indicating that the TiO₂ layer acted as a corrosion inhibitor.^[82] In addition, He et al. demonstrated the preparation of an ultra-thin Al₂O₃ protective coating on a zinc anode by ALD for dendrite-free zinc deposition. The corrosion potentials of bare Zn and Al₂O₃@Zn are -871.1 mV and -875.7 mV (vs. Ag/AgCl), which further confirms the corrosion resistance of Al₂O₃ coating.^[83] Some polymers also have anti-corrosion effects, and polyamide (PA)-based AEI is designed to protect zinc metal anodic PA coatings. The polar amide group on the PA chain can interrupt the solvation sheath of Zn²⁺ in the interphase by forming hydrogen bonds with water molecules, and the corrosion resistance of the coated anode is significantly enhanced (Figure 7g and h).^[84] Guo et al. uniformly deposited a PVB butanal film on the Zn surface by a simple spin coating strategy. Linear polarization experiments in 1 M ZnSO₄ show that compared with bare zinc electrode, the corrosion potential of PVB galvanized electrode increases from -1.052 to -1.010 V due to PVB passivation coating, which effectively inhibits the interface corrosion.^[85]

3.2. Hydrophobic layer shielding

In aqueous electrolyte solutions, H₂O has a complex chemical environment: either strongly coordinated with cations or weakly coordinated with anions, or roaming freely in the electrolyte. The thermodynamic method of inhibiting hydrogen evolution is to reduce the activity of water significantly. According to the Nernst equation, the logarithm of the activity is linear to the potential of the electrochemical reaction.^[86] This means that water molecules are less active, making it harder to oxidize or reduce water molecules. The hydrophobic interface layer will physically prevent water molecules from reaching the electrode interface and reduce the water activity at the interface to solve the problem from the raw material source of

hydrogen evolution reaction. At present, there are usually two methods to construct the superhydrophobic interface: 1) modify the low surface energy material on the surface with micro or nano rough structure; 2) construct micro-nano rough structures on the surface of materials with low surface energy.

Alkyl ammonium salts can form fluorinated hydrophobic interphase on the surface of the zinc anode in situ. Such AIL inhibits H₂ evolution and increases the electrochemical stability window of the electrolyte.^[24] Wang et al. introduced NO₃⁻ into the electrolyte to generate a passivation layer on the zinc surface in situ. In the subsequent cycle, the passivation layer gradually transformed into an organic layer dominated by Zn(CO₃)₂(OH)₆ and an inorganic layer dominated by ZnF₂ (Figure 8a). The hydrophobic organic layer was shielded from precipitation molecules, and they built their own hydrogen detection system using a chromatograph to quantify the hydrogen in circulation.^[87] Considering the hydrophobic ability of polymers, Pu et al. coated the porous zinc surface with a layer of PTFE and used its hydrophobicity to prevent water molecules from reaching the electrode surface to decompose (Figure 8b).^[88] Xin et al. constructed a layer of hydrophobic polystyrene molecular brush with a thickness of only 6.5 nm on the surface of the Zn. The molecular brush was combined with the Zn substrate through the chemical dehydration reaction between the hydroxyl group, and the resulting molecular brush interface layer has the characteristics of single layer and small thickness. It is important that one end of the molecular brush away from the Zn metal substrate has hydrophobic groups, so the molecular brush interface film can block the infiltration of water molecules to a certain extent.^[89] Lee et al. described ionic liquid (IL) gels as a waterproof ionic conductive protective layer customized for zinc anodes by ultraviolet (UV) curing, which consists of a hydrophobic ionic liquid solvent (BMPTFSI), a zinc salt (Zn(TFSI)₂), and a thiol-ene polymer-compatible skeleton. BMP⁺ cation is hydrophobic in BMPTFSI, which can effectively shield water molecules and inhibit its decomposition. The results show that the IL thin gel can effectively inhibit the water-induced parasitic reaction at the interface with the zinc electrode and achieve dendrite-free plating/stripping (Figure 8c and d).^[90]

3.3. Channel limited domain desolvation

In addition, it has been pointed out that desolvent treatment of solvated metal ions at the negative electrode interface can effectively inhibit or even eliminate the side reactions caused by water. (Figure 9a).^[91] Solvated metal ions remove the solvated shell in a process similar to the use of channels smaller than the original material to screen out unwanted parts. Most of the solvated metal ions are at the sub-nanometer scale, so the screening of additional solvent molecules requires pores with sub-nanometer sieving capabilities. In addition, in order to increase the transport of Zn²⁺ and remove the solvated shell more effectively, appropriate groups can be modified in the pores, and the physical and chemical interactions between

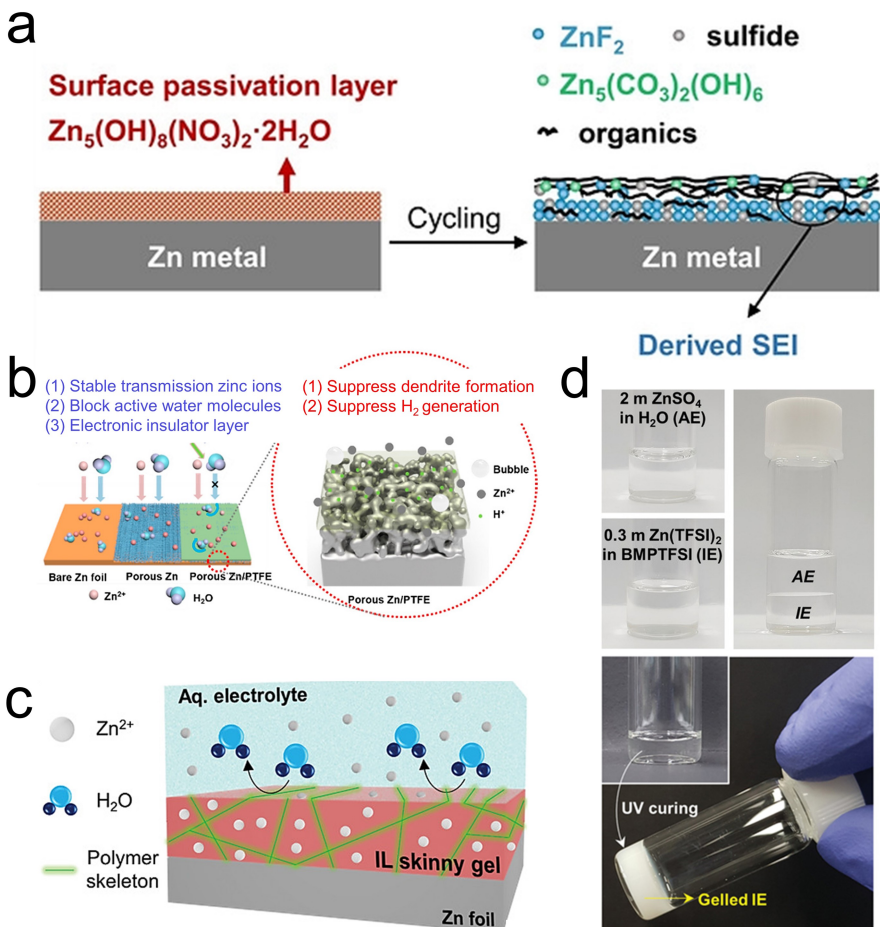


Figure 8. a) The presence of NO_3^- promotes the formation of a schematic diagram of an inorganic layer with ZnF_2 inside and an organic layer with $\text{Zn}_5(\text{CO}_3)_2(\text{OH})_6$ outside. Reproduced with permission from Ref. [87]. Copyright (2021) Wiley-VCH. b) Schematic diagram of the reaction process on porous Zn and porous Zn/PTFE. Reproduced with permission from Ref. [88]. Copyright (2022) American Chemical Society. c) The diagram depicts an IL thin gel on a zinc anode as a waterproof protective layer. d) Optical photograph of AE and IE electrolyte phase separation (top). Photographs of the IL gel before and after UV curing-driven solidification (bottom). Reproduced with permission from Ref. [90]. Copyright (2021) Wiley-VCH.

them and ions can be used to further improve the desolvation effect.

Some of the water molecules can be shielded porous screening, so as to inhibit the activity of free water, such as: molecular sieve unique pore structure can be ruled out, a certain amount of water molecules lead to changes in zinc ions coordination environment, conducive to the formation of local high concentration of electrolyte, prevent reactive H_2O molecules, direct contact with zinc metal so as to curb its ehrs, corrosion and by-products.^[50] Zhou et al. prepared a ZnO functional layer with a 3D porous structure on the surface of the metal zinc negative electrode. Zn@ZnO-3D Geometrically optimized O elements can clearly induce additional charge concentration at the surface. Zn^{2+} can be preferentially adsorbed and easily bound to reduce the binding of zinc hydrate ions. Thus, this nicely results in electrostatic attraction to Zn^{2+} rather than solvated or hydrated Zn^{2+} , thus reducing the free water of the strong and tight solvated sheath near the zinc metal, effectively preventing H_2 evolution.^[92] In Nafion film, due to the presence of 4 nm channels, Zn^{2+} , SO_4^{2-} and free water can be transmitted to the surface of the Zn anode

through the channels, resulting in side reactions. However, for the Nafion-Zn-X film layer, Zn-X forms a tight organic-inorganic composite interface through bridging between Zn^{2+} and sulfonic acid groups in Nafion, and free water molecules can only penetrate through Zn-X. However, the X-zeolite channel (0.74 nm) is much smaller than the Nafion channel (4 nm), so it can greatly inhibit the penetration of sulfate and free water and reduce side reactions (Figure 9b).^[93] In addition, Wang et al. constructed a homogeneous ZCO layer with a unique three-dimensional frame structure and nucleophilic carbonyl group on the surface of zinc, as shown in Figure 9(c). The hydrogen bond network formed by the oxygen atom as the proton acceptor in Zn@ZCO can regulate the desolvation process of zinc ions. The abundant hydrophile groups and charge groups can effectively restrict the water molecules in the zinc oxalate frame structure, thus reducing the side reactions caused by water. The battery also shows excellent electrochemical performance.^[94]

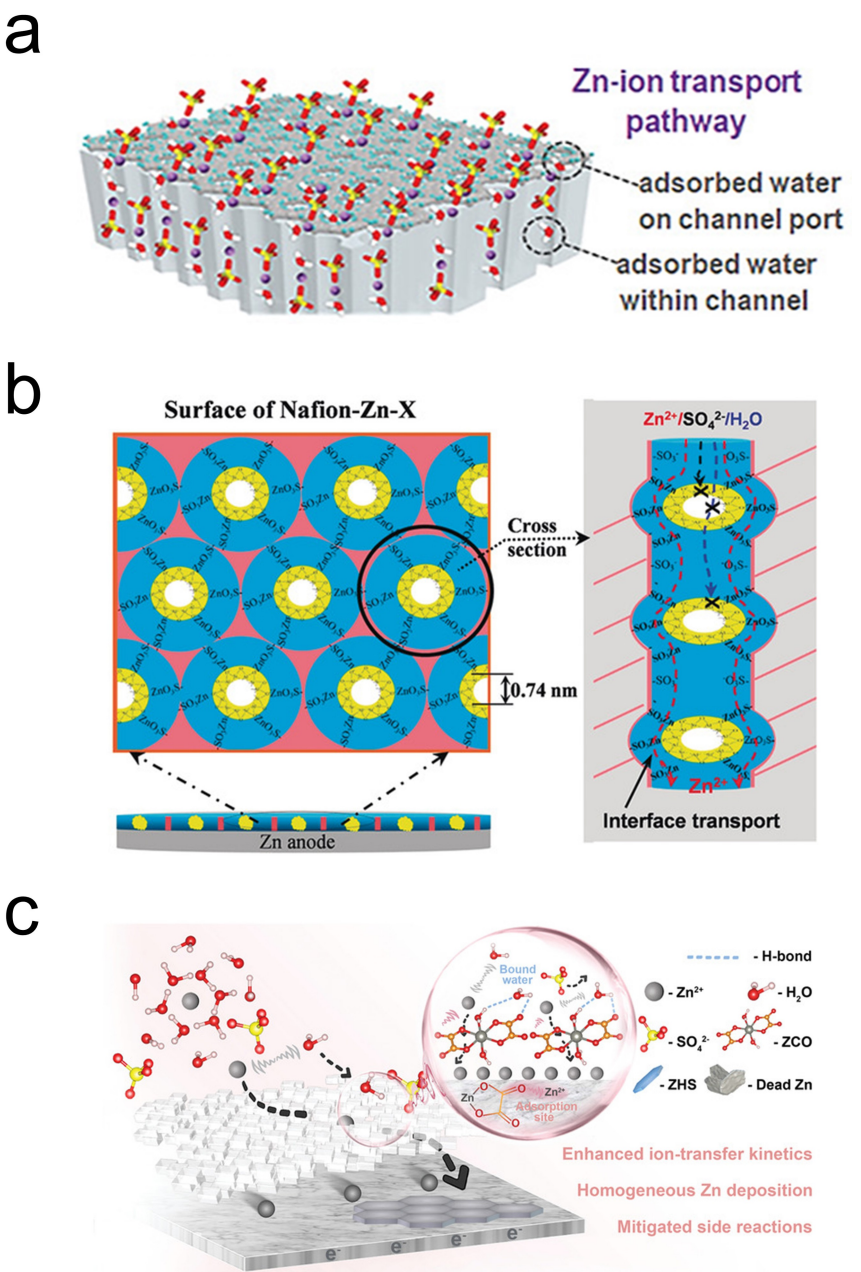


Figure 9. a) The existence of water absorbed inside and bonded in the surface of zeolite can facilitate the ion transport of Zn²⁺. Reproduced with permission from Ref. [91]. Copyright (2022) Wiley-VCH. b) Ion transport mechanisms in Nafion-Zn-X protective layers. Reproduced with permission from Ref. [93]. Copyright (2020) Wiley-VCH. c) Schematic illustration of Zn deposition on Zn@ZCO electrodes. Reproduced with permission from Ref. [94]. Copyright (2022) Wiley-VCH.

3.4. Counter catalyst regulation

From the kinetic point of view, the ideal aqueous electrode interface in the inhibition strategy of hydrolysis should be a good anti-electrolytic catalyst and provide a high electrochemical overpotential for HER process. The adsorbed hydrogen atom forms M–H* bond with the electrode surface through a single electron transfer process (Figure 10a). The adsorbed H* atoms are reduced by Heyrovsky or Tafel reactions to form H₂ molecules, which are finally desorbed from the electrode surface.^[76,95] Kinetic inhibition of hydrogen evolution is based

on the principle of reverse catalysis. It is necessary to increase the activation energy of hydrogen evolution reactions and reduce the rate of these reactions, thus reducing the effect of hydrogen evolution (Figure 10b).^[96]

The Gibbs free energy ΔG_{H^*} , which adsorbs H atoms to form H₂, is a key descriptor for predicting and evaluating HER surface activity.^[97] The adsorption step limits the overall kinetics and determines the weak binding strength ($\Delta G_{H^*} > 0$), while the electrochemical overpotential of the desorption step is at a lower binding energy ($\Delta G_{H^*} < 0$). Lower dominance. Theoretically, the closer ΔG_{H^*} is to 0 eV, the stronger HER activity is, the

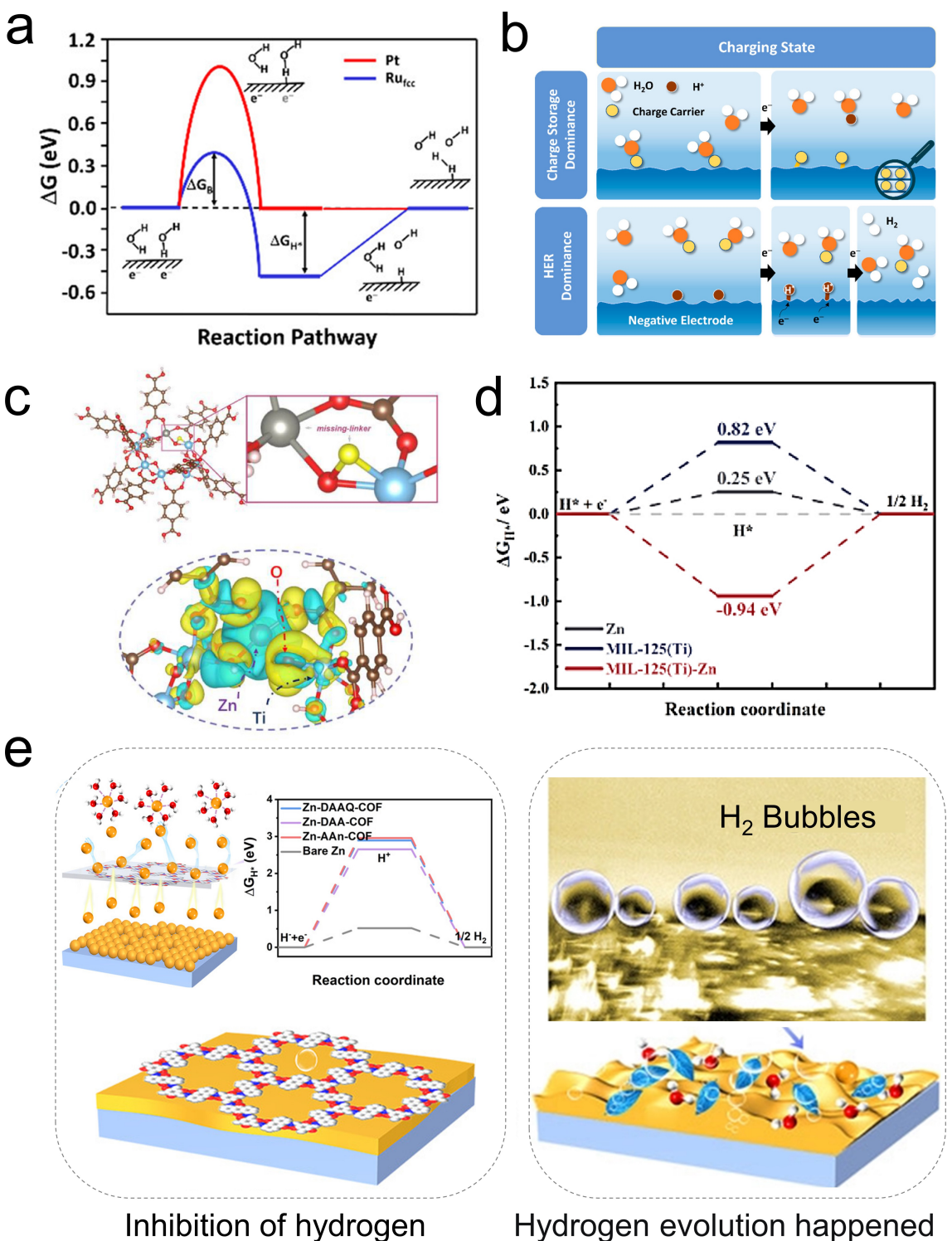


Figure 10. a) Gibbs free energy diagram of the HER process in order of initial state of reactants, hydrolysis dissociation state, intermediate state, and product state. Reproduced with permission from Ref. [97]. Copyright (2016) American Chemical Society. b) Schematic diagram of the competitive route between HER and redox reactions on the anode electrode during charging. Reproduced with permission from Ref. [96]. Copyright (2021) American Chemical Society. c) Schematic diagram of structure and differential charge density of MIL-125(Ti)-Zn. d) Free energy plots of HER on Zn(001), MIL-125(Ti) and MIL-125(Ti)-Zn. Reproduced with permission from Ref. [99]. Copyright (2022) Elsevier. e) Zn-COF@Zn Schematic diagram of surface inhibition of hydrogen evolution (left). Schematic diagram of hydrogen evolution on bare zinc surface to produce bubbles (right). Reproduced with permission from Ref. [100]. Copyright (2022) Wiley-VCH.

more conducive to hydrogen precipitation. On the contrary, the larger the absolute value of ΔG_{H^*} , the weaker HER activity

and the more difficult it is to precipitate hydrogen.^[76,98] Zhi et al. calculated the Gibbs free energy ΔG_{H^*} on Zn(002) and

ZnF₂ side, and the ΔG_{H^*} value at Zn@ZnF₂ interface was 1.31 eV, much higher than Zn (1.00 eV) and Pt(111) reference (0.04 eV).^[23] Therefore, they confirmed that the ZnF₂ interface structure can greatly inhibit hydrogen evolution reaction. Zhang et al. constructed a linome-missing MOF material MIL-125(Ti)-Zn as an AIL. The Zn-incorporated missing linker structure in MIL-125(Ti) can regulate the electronic states of Ti and O and construct electron-rich oxygen sites by increasing the electron density of oxygen (Figure 10c).^[99] Figure 10(d) shown that the ΔG_{H^*} value of the oxygen-rich site is 0.82 eV, which enhances the adsorption of HER intermediate H* on the surface, and thus inhibits the side reaction of hydrogen evolution on the negative electrode of zinc metal. Lan proposed two-dimensional COFs as artificial coatings. In order to quantify the hydrogen precipitation process accurately, the hydrogen precipitation process was monitored by cell gas chromatograms mass spectrometry (GC-MS), and the hydrogen evolution amount was measured (0.002 mmol h⁻¹ cm⁻², which was two orders of magnitude smaller than that of pure zinc foil). The ΔG_{H^*} value of COF@Zn (2.94 eV) is six times higher than that of bare zinc, indicating that its weak adsorption capacity for H* could provide a more difficult hydrolysis dissociation process, thus effectively inhibiting H₂ evolution (Figure 10e).^[100] In addition, the famous volcano diagram in heterogeneous catalysis is very instructive, the relatively poor catalyst is at the foot of the volcano. In the search for counter-catalysts, the material at the foot of the volcano in these volcanic images can be studied. Therefore, the application of artificial interface protective layer in counter catalysis still has great development space.

In general, AIL inhibition of HER is still in the research stage. For the future development, more attention should be transferred to the interaction between interface engineering and electrolyte engineering, so that the artificial interface layer can play a greater role. In water environment, the presence of hydrogen evolution corrosion reaction requires AIL to be more robust than the SEI in aprotic cells. Therefore, it is also crucial to study the durability of SEI in different states.

4. Principle III: Excellent Mechanical Stability

Unlike the enhancement of ion conductivity, homogeneity, and passivation inhibition of hydrogen evolution, the mechanical properties of artificial interfacial layers have rarely been studied on the battery and are generally considered as an additional advantage. However, an increasing number of studies have found that mechanical properties are also one of the key properties for obtaining high cycle efficiency of metallic zinc anodes. Zn dendrite growth mechanism by material thermodynamics, dynamics (ionic conductivity, exchange current density), mechanical properties (stiffness, interfacial toughness), the influence of Zn anode in the process of repeated cycle of interface changes greatly and produce the dendrite problem, so the interface layer should be high enough toughness and mechanical stability. High toughness can withstand volume changes, high mechanical stability can avoid fracture failure.

There are two main directions for designing mechanical properties of interfacial layer materials. One way is to make the mechanical strength or hardness of the interfacial layer as high as possible. The increase of shear modulus of the artificial interface layer can cause dendrite plastic deformation and make the interface flat. Another design direction is to screen suitable soft materials to adapt to the volume change of metal deposition in a flexible way to avoid damage caused by protective layer failure and poor electrode contact.

4.1. Improve the mechanical strength of AIL

For a rugged AIL, high mechanical strength is required to withstand high stress variations and penetration. Initially, Barton and Bockris identified surface tension as the driving force for dendrite growth by studying the formation and growth rates of silver dendrites.^[101] Based on the surface tension theory, Diggle et al. studied the growth of zinc dendrites in alkaline electrolyte in detail, and expounded the influence of deposition overpotential on dendrite growth.^[102] Yamaki et al. proposed that the dendrite generation was due to SEI fracture caused by the stress generated when lithium was deposited under SEI.^[103] Monroe and Newman considered the effects of elasticity, viscosity, and applied pressure, and proposed that polymer electrolytes with high shear modulus could effectively inhibit dendrite growth. Theory predicts that the shear modulus of electrolyte should be at least twice higher than that of metal to effectively inhibit dendrite growth.^[104] Viswanathan analyzed the effect of electrolyte on the zinc negative electrode by establishing a nonlinear phase field model of electrodeposition. The model considers the contribution of mechanical energy to the chemical potential and finds that the dendrite length is shorter when the modulus of the electrolyte is higher. Figure 11(a) shows that when the product modulus of the electrolyte is greater than 6.7 GPa, dendrite growth is greatly inhibited. In the extreme case where the modulus is greater than 66.7 GPa, the interface is smooth due to the large mechanical inhibition effect.^[105]

Inorganic materials have been widely concerned as artificial protective layer due to their high mechanical stiffness. Using acetamide/Zn(TFSI)₂ low eumelt electrolyte, Cui et al. successfully constructed an *in situ* SEI film on the zinc anode surface for the first time (Figure 11b).^[106] Cao et al. reported a strategy of forming fluorinated interfacial layers promoted by electrolyte additives. Because fluorine compounds themselves are species with high shear modulus and high interfacial energy to zinc, AIL can withstand the large elastic stress caused by the large volume change of zinc anode during charging and discharging, and maintain the structural integrity during multiple cycles.^[24] Zhao et al. calculated ZnF₂ has 100 GPa mechanical modulus.^[26] The ZnS film exhibits strong adhesion, good mechanical strength and high ionic conductivity.^[28] Jiang et al. prepared double-layer diamond-like ZnS (DLC-ZnS) films by RF magnetron sputtering. The mechanical properties of the films were investigated by bimodal FM-AM atomic force microscopy (Figure 11c). The Young's modulus of DLC films was 95 GPa

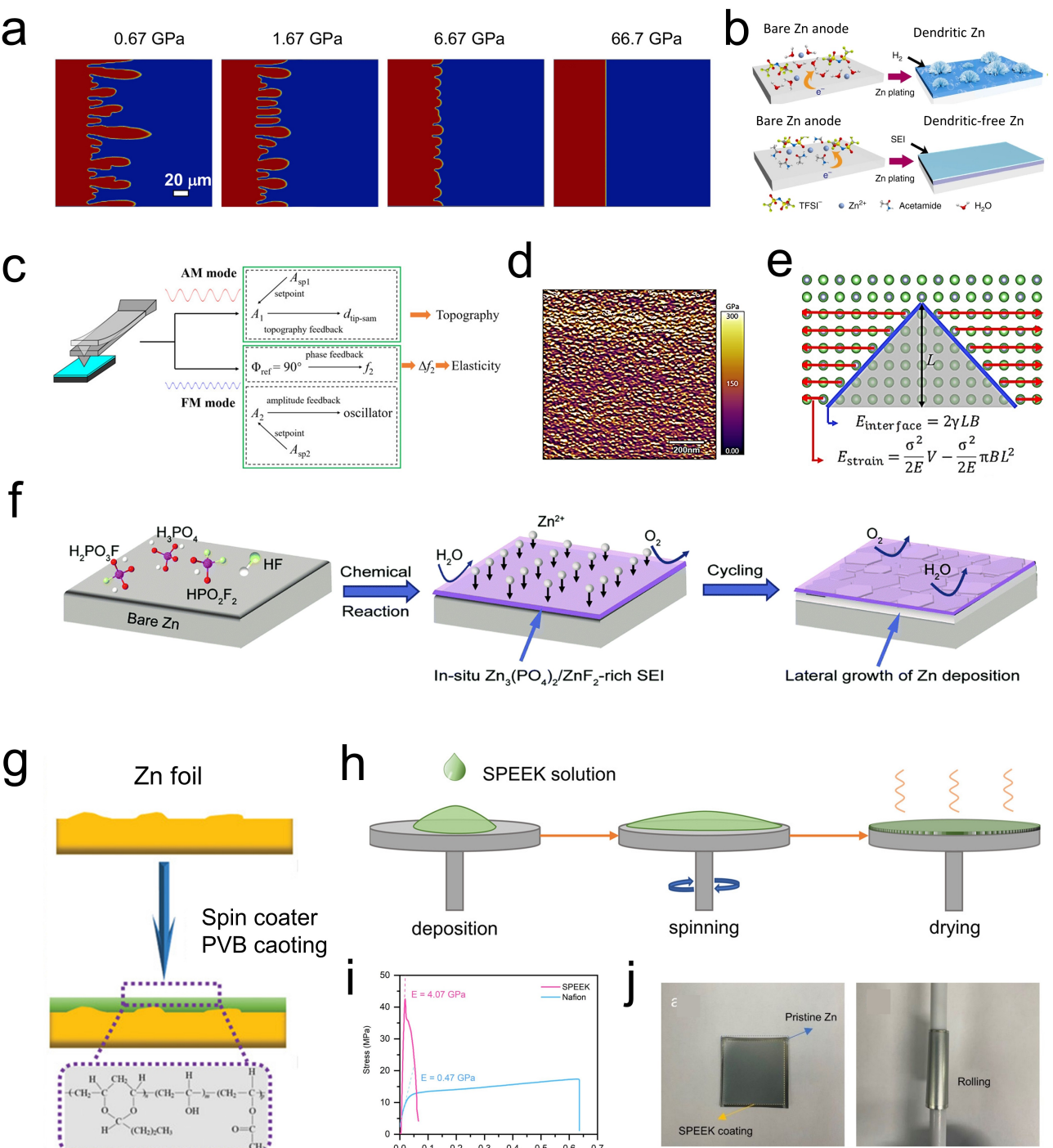


Figure 11. a) A nonlinear phase field model for zinc electrodeposition. Reproduced with permission from Ref. [105]. Copyright (2020) American Chemical Society. b) The electrolyte additive forms a fluorinated interfacial layer with high shear modulus. Reproduced with permission from Ref. [106]. Copyright (2019) Springer Nature. c) Test of mechanical properties of thin films by bimodal frequency-modulated AFM. d) AFM topographic and phase images and Young's modulus of DLC-ZnS. Reproduced with permission from Ref. [107]. Copyright (2020) American Chemical Society. e) Criteria for dendrite inhibition by metal/SEI interfacial energy (γ) and component bulk modulus (E). Reproduced with permission from Ref. [108]. Copyright (2018) AAAS. f) In situ built $\text{Zn}_3(\text{PO}_4)_2/\text{ZnF}_2$ interphase for Zn metal. Reproduced with permission from Ref. [109]. Copyright (2021) Royal Society of Chemistry. g) Dense PVB films were prepared on Zn surface. Reproduced with permission from Ref. [85]. Copyright (2020) Wiley-VCH. h) The protective layer of SPEEK was prepared by spin coating. i) SPEEK and Nafion stress-strain curve. j) SPEEK binds strongly to Zn. Reproduced with permission from Ref. [112]. Copyright (2021) American Chemical Society.

higher than that of ZnS films (70 GPa) (Figure 11d).^[107] High modulus DLC films significantly enhance the mechanical strength of the interface, and further improve the reversible

capacity and cycling stability. The combination of metal/SEI interfacial energy (γ) and component volume modulus (E) is considered as a criterion for evaluating dendrite inhibition

ability of SEI layers, as shown in Figure 11(e).^[108] Inspired by this theory, Luo et al. used density functional theory to calculate the interfacial energy and bulk modulus between zinc and four inorganic compounds (ZnO , Zn(OH)_2 , ZnF_2 , and $\text{Zn}_3(\text{PO}_4)_2$). $\text{Zn}_3(\text{PO}_4)_2$ has a high interfacial energy of 357.72 meV A^{-2} and a bulk modulus of 98.88 GPa, and the highest γE value shows a unique ability to inhibit the dendrite growth of Zn (Figure 11f).^[109]

In addition, some special polymers and inorganic-polymer composites with high mechanical strength have also been reported as protective layers. For example, poly(3,4-ethylene dioxythiophene): polystyrene sulfonate (ZPS) is cross-linked by Zn^{2+} in situ to form a hybrid electron/ion conductor interface on the Zn metal surface. The ultimate tensile strength of ZPS layer is 46.3 MPa and Young's modulus is 1.47 GPa.^[110] Guo et al. prepared a dense PVB film as an AIL for the zinc anode (Figure 11g). The Young's modulus of PVB films measured by AFM is 220–260 MPa, showing a certain mechanical strength to inhibit the growth of Zn dendrites.^[85] Qie et al. introduced an elastic confinement layer (AEC) composed of PVDF matrix decorated with titanium dioxide nanoparticles. The average elastic modulus of AEC obtained by nano-indentation machine is 2.67 GPa, with good mechanical flexibility to provide elastic confinement to alleviate interfacial reactions.^[111] An ultra-thin (~1 μm) SPEEK AIL was constructed on Zn anode by a simple spin coating (Figure 11h). The mechanical strengths of SPEEK and Nafion were measured and compared by strain-stress curve. Figure 11(j) shows that the Young's modulus of SPEEK was found to be as high as 4.3 GPa, order of magnitude higher than the Young's modulus of Nafion polymer (0.4 GPa).^[112] Later, Wang et al. used solid UIO-66 as nano-filler and flexible SPEEK adhesive (USL) for artificial SEI film, and the Young's modulus of USL film was detected by AFM to be 8.63 GPa, nearly double that of SPEEK alone. The mechanical strength of this USL film should come from the integration of mechanically rigid MOF nanospheres and elastic flexible SPEEK adhesive.^[39] According to the theoretical prediction, the mechanical modulus of layers is far from enough to completely inhibit the growth of dendrites, so efforts should be continued to find high mechanical modulus.

4.2. Dynamic adaptive interface

In addition, due to poor flexibility and mechanical wettability, the rigid solid electrolyte interface will lead to uneven contact at the local interface after contact with the metal. The uniform contact between the interface layer and the negative interface of the zinc metal is essential for the uniform distribution of the current density. In order to avoid mechanical failure of the membrane, it is important to develop a coating with adaptive interfacial volume change, strong adhesion and rapid self-healing effect. Soft materials are usually amorphous polymers without serious grain boundary defects and can completely cover the metal surface. This unique property allows soft polymers to adapt to large volume changes during the cycling of metal electrodes.

Some soft polymers have advantages that hard materials do not, such as self-healing properties. When mechanical damage occurs to the interface layer during circulation, self-healing materials can be quickly repaired to avoid failure. Qie et al. designed a self-healing protective layer rich in amide bonds and ether bonds to stabilize the Zn anode (Figure 12a). The AIL consisted of three parts: self-healing site, cross-linking unit and flexible chain segment. Due to the unique advantages of hydrogen bonds between molecules, the coating shows excellent self-healing ability, which can repair mechanical cracks generated during the cycling process.^[113] Many hydrogels have self-healing effect, but are limited by water absorption and swelling, so self-healing design is mostly used in the design of solid electrolytes.^[114]

Due to the long chain structure of polymer macromolecules and the nature of polymer movement, the deformation and flow of polymer cannot be purely elastic and viscous. The stress response has the dual characteristics of an elastic solid and a viscous fluid, which is called viscoelastic. In the field of Li metal, some attempts have been made. Zheng et al. applied self-healing viscoelastic polymer coatings to lithium metal anodes and showed great performance improvement.^[115] Kong et al. theoretically simulated polymer coatings with different mechanical properties and found that viscoelastic polymers generally inhibited Li dendrites more effectively than hard coatings with distinct grain boundaries and defects (Figure 12b).^[116] Wei et al. provided experimental and theoretical evidence that viscoelastic liquid electrolytes can stably electro-deposit many metals.^[117] Cui et al. coated multifunctional polyamide (PA) and $\text{Zn}(\text{TfO})_2$ protective coatings on Zn. The dynamic thermodynamic analysis experiments show that the PA layer is able to maintain sufficient viscoelasticity and flexibility to adapt to the mechanical stresses generated during cycling.^[84] Guo et al. developed a highly adaptive PDMS (polydimethylsiloxane)/ TiO_{2-x} coating, which can dynamically adapt to volume changes and uniformly deposit zinc ions, providing an effective guarantee for stable operation of the metal zinc anode. Figure 12(c) shows that the synthetic PDMS has viscoelastic mechanical characteristics due to the micro-cross-linking of B–O bonds, which endows them with high dynamic adaptability.^[118]

However, this kind of research is rare at present, which can be inspired from electrolyte research. For example, Shear thickened fluid (STF) is a kind of non-Newtonian fluid, the relationship between shear stress and shear strain rate is not linear. In the absence of applied force, the STF exhibits deformable behavior and flows like a liquid. However, its viscosity increases rapidly with the shear rate, and beyond the shear rate threshold it becomes a very hard solid material. Starch has been used to develop a new electrolyte with both liquid and solid behavior to increase cycling stability and improve the morphology of zinc metal anodes. When the electrolyte is deposited inhomogeneous locally, mechanical hardening occurs in the region of rapid Zn growth to inhibit local dendrite growth, as shown in Figure 12(d).^[119] Thus, Zn plating/stripping in NNFE with dynamic "solid-liquid" transitions can be run reversibly and stably for 20,000 cycles at

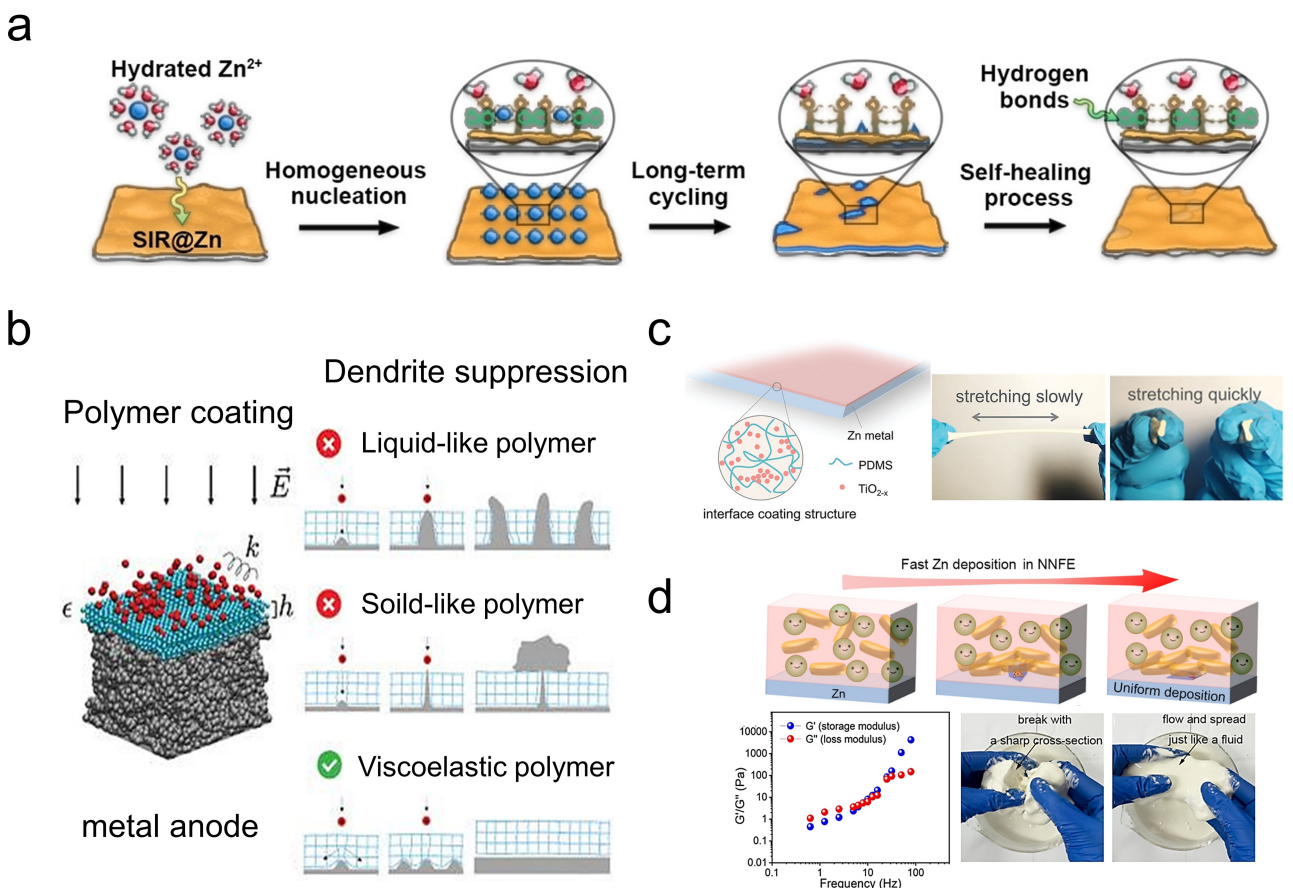


Figure 12. a) The schematic diagrams showing the structural evolution of SIR@Zn and Zn electrodes during cycling. Reproduced with permission from Ref. [113]. Copyright (2022) Wiley-VCH. b) Schematic diagram of the effect of different polymer mechanical properties on the growth and morphology of nucleated dendrites. Reproduced with permission from Ref. [116]. Copyright (2020) Wiley-VCH. c) Schematic diagram of interface coating. And optical photos of slow stretching, fast stretching. Reproduced with permission from Ref. [118]. Copyright (2022) Wiley-VCH. d) The schematic illustration of Zn dendrite growth in non-Newtonian fluid(NNFE). Rheological study of NNFE. Digital image of cross section of NNFE at high rate tensile showing hardened fracture. Reproduced with permission from Ref. [119]. Copyright (2022) American Chemical Society.

extremely high rates up to 50 mA cm^{-2} . Similarly, He developed a colloidal electrolyte strategy using cornstarch to enhance the intrinsic impact resistance of electrolytes.^[120]

The interface protection layer needs to have certain mechanical properties to resist the volume change of electrode material during the cycle and the pressure generated in the subsequent cell preparation process, which also puts forward new requirements on the hardness, stiffness and strength of the protection layer. Brittle materials are very prone to crack or even fracture under the action of these stresses. The soft material with low hardness, low modulus and low fracture toughness is conducive to accommodating the volume change of the pole sheet and ensure the stability of the interface structure to avoid failure. The above interface protective layer has some contradictory requirements on mechanical properties. For example, high shear modulus is conducive to inhibiting dendritic growth, but not conducive to maintaining tight interfacial contact. Therefore, the evaluation of the mechanical properties of the interface protective layer should be considered comprehensively to balance the advantages and disadvantages of each factor.^[121]

5. Conclusion and Outlook

In this review, we have identified several key properties of Zinc-metal interfacial layer. Rapid and uniform ion transport, mitigation of corrosion and hydrogen evolution side reactions, and improve mechanical stability are the three most important aspects for the success of artificial interface layer design. In short, it is expected that through the guidance of these theoretical principles to better design the interface protection layer in line with the practical application, in order to achieve the stability of metal zinc anode and achieve the purpose of practical application.

In order to achieve cheap and safe rechargeable battery systems, the performance metrics at the electrode level should be more carefully evaluated, and eventually extended to the battery level in order to achieve higher weight or volume energy densities. For example, complex ALIs with multiple functional roles are a priority for future applications, and a properly designed artificial interface layer should also have high ionic conductivity ($> 10^{-4} \text{ Scm}^{-1}$ or even 10^{-3} – 10^{-2} Scm^{-1}), single ion transport ($t_+ \approx 1$), ideal mechanical properties ($> 108 \text{ Gpa}$, super defect free or adaptive) and the

ability to mitigate side effects. In addition, the evaluation should include the cyclic stability of the positive electrode at the normal discharge rate ($\geq 1 \text{ A g}^{-1}$) and the actual volume ($\geq 5 \text{ mAh cm}^{-2}$). The energy density and volumetric energy density are also evaluated when controlling the volume (N/P) ratio between the negative and positive electrodes, taking zinc utilization into account. More importantly, in order to evaluate the cycle performance of zinc-ion batteries more realistically, full-battery performance with an N/P ratio of less than 3 was tested. In assessing progress in this area, much of the literature does not show much cost analysis and zinc utilization or mass energy density of the battery as a whole, let alone power density or volume capacity of the system. The field is still in its infancy. These are important indicators for the future development of zinc-ion batteries.

The thermo-electrochemical stability window of water is 1.23 V and is related to the solvent and salt components in the electrolyte. Oxygen evolution reaction (OER) and hydrogen evolution reaction (HER) are easy to cause electrolyte decomposition, which can not be ignored. OER reaction limits the selection of anode materials and the increase of voltage. HER reaction affects the cycle life of Zn anode. Therefore, the artificial interface layer strategy should be developed in collaboration with electrolyte engineering to improve the voltage stability of the aqueous electrolyte of Zn batteries, so as to improve the overall cycle life of zinc ion batteries.

In addition, battery system is a complex and nonlinear system, which requires the coupling analysis of electrochemical-thermo-mechanical and other disciplines. Although the material development of the interfacial layer is a research hotspot, the theoretical model that plays a guiding role is still stagnant and has not been developed greatly. For example, the traditional conduction mechanism of ionic conductors considers that in inorganic materials, ions are transferred by movement at defects, while in polymers, they are transferred by jumping between oxygen-containing column segments. However, the radius and solvation atmosphere of polyvalent metal ions are different from those of alkali metal ions. Although the transport mechanism of polyvalent metal ions can be used for reference, the exact and detailed migration path needs further study. In terms of the mechanical properties of the coatings, the shear modulus criteria proposed by Monroe and Newman apply only to polymeric electrolytes and solid-state electrolyte systems without any inhomogeneity or defects. This is not consistent with the change of the interface of zinc anode under actual working conditions, and more mechanical properties need to be further studied.

Therefore, similar to the multivalent metal ion transport model, electrochemical and mechanical coupling model, counter-catalytic model and other theoretical research with the progress of science and technology need to put forward new insights. In addition, the coupling relationship between multiple physical fields should be actively explored to better guide the design of artificial interface layer in the future.

Acknowledgements

This work was supported by the Natural Science Foundation of Heilongjiang Province (No. LH2020B008), the Heilongjiang Postdoctoral Funds for Scientific Research Initiation (LBH-Q21015).

Conflict of Interest

The authors declare no conflict of interest.

Keywords: zinc anode · dendrites · hydrogen evolution · battery · artificial interface layer

- [1] a) W. A. Braff, J. M. Mueller, J. E. Trancik, *Nat. Clim. Change* **2016**, *6*, 964–969; b) A. E. MacDonald, C. T. M. Clack, A. Alexander, A. Dunbar, J. Wilczak, Y. Xie, *Nat. Clim. Change* **2016**, *6*, 526–531.
- [2] a) N. Zhang, T. Deng, S. Q. Zhang, C. H. Wang, L. X. Chen, C. S. Wang, X. L. Fan, *Adv. Mater.* **2022**, 2107899; b) L. Ji, Z. Lin, M. Alcoutlabi, X. Zhang, *Energy Environ. Sci.* **2011**, *4*, 2682–2699; c) T. Wei, N. Zhang, Y. Ji, J. Zhang, Y. Zhu, T. Yi, *Chin. Chem. Lett.* **2022**, *33*, 714–729.
- [3] a) O. Schmidt, A. Hawkes, A. Gambhir, I. Staffell, *Nat. Energy* **2017**, *2*, 17110; b) S. Yang, F. Zhang, H. Ding, P. He, H. Zhou, *Joule* **2018**, *2*, 1648–1651; c) T.-F. Yi, L.-Y. Qiu, J. Mei, S.-Y. Qi, P. Cui, S. Luo, Y.-R. Zhu, Y. Xie, Y.-B. He, *Sci. Bull.* **2020**, *65*, 546–556.
- [4] a) X. Zeng, K. Xie, S. Liu, S. Zhang, J. Hao, J. Liu, W. K. Pang, J. Liu, P. Rao, Q. Wang, J. Mao, Z. Guo, *Energy Environ. Sci.* **2021**, *14*, 5947–5957; b) C. Ding, C. Li, H. Tian, Y. Tong, W. Huang, Q. Zhang, *Batteries & Supercaps* **2022**, *5*, e202200160.
- [5] a) B. Tang, L. Shan, S. Liang, J. Zhou, *Energy Environ. Sci.* **2019**, *12*, 3288–3304; b) R. Zhao, H. Wang, H. Du, Y. Yang, Z. Gao, L. Qie, Y. Huang, *Nat. Commun.* **2022**, *13*, 3252; c) T.-F. Yi, L. Qiu, J.-P. Qu, H. Liu, J.-H. Zhang, Y.-R. Zhu, *Coord. Chem. Rev.* **2021**, *446*, 214124.
- [6] a) X. Guo, Z. Zhang, J. Li, N. Luo, G.-L. Chai, T. S. Miller, F. Lai, P. Shearing, D. J. L. Brett, D. Han, Z. Weng, G. He, I. P. Parkin, *ACS Energy Lett.* **2021**, *6*, 395–403; b) L. Hong, X. Wu, C. Ma, W. Huang, Y. Zhou, K.-X. Wang, J.-S. Chen, *J. Mater. Chem. A* **2021**, *9*, 16814–16823; c) F. Ming, Y. Zhu, G. Huang, A. H. Emwas, H. Liang, Y. Cui, H. N. Alshareef, *J. Am. Chem. Soc.* **2022**, *144*, 7160–7170.
- [7] a) S. S. Shinde, J. Y. Jung, N. K. Wagh, C. H. Lee, D.-H. Kim, S.-H. Kim, S. U. Lee, J.-H. Lee, *Nat. Energy* **2021**, *6*, 592–604; b) Y. Zhu, Y. Cui, H. N. Alshareef, *Nano Lett.* **2021**, *21*, 1446–1453; c) C. Lin, S.-H. Kim, Q. Xu, D.-H. Kim, G. Ali, S. S. Shinde, S. Yang, Y. Yang, X. Li, Z. Jiang, J.-H. Lee, *Matter* **2021**, *4*, 1287–1304; d) F. Wang, O. Borodin, T. Gao, X. Fan, W. Sun, F. Han, A. Faraone, J. A. Dura, K. Xu, C. Wang, *Nat. Mater.* **2018**, *17*, 543–549.
- [8] a) J. Zheng, Q. Zhao, T. Tang, J. Yin, C. D. Quilty, G. D. Renderos, X. Liu, Y. Deng, L. Wang, D. C. Bock, C. Jaye, D. Zhang, E. S. Takeuchi, K. J. Takeuchi, A. C. Marschilok, L. A. Archer, *Science* **2019**, *366*, 645–648; b) W. Du, J. Yan, C. Cao, C. C. Li, *Energy Storage Mater.* **2022**, *52*, 329–354.
- [9] Y. Shang, D. Kundu, *Batteries & Supercaps* **2022**, *5*, e202100394.
- [10] Z. Yi, G. Chen, F. Hou, L. Wang, J. Liang, *Adv. Energy Mater.* **2021**, *11*, 2003065.
- [11] a) N. Dong, X. Zhao, M. Yan, H. Li, H. Pan, *Nano Energy* **2022**, 107903; b) H. Wang, H. Li, Y. Tang, Z. Xu, K. Wang, Q. Li, B. He, Y. Liu, M. Ge, S. Chen, T. Hao, G. Xing, Y. Zhang, *Adv. Funct. Mater.* **2022**, 2207898; c) N. Wang, X. Dong, B. Wang, Z. Guo, Z. Wang, R. Wang, X. Qiu, Y. Wang, *Angew. Chem. Int. Ed.* **2020**, *59*, 14577–14583; *Angew. Chem.* **2020**, *132*, 14685–14691.
- [12] a) Y. Xu, X. Zheng, J. Sun, W. Wang, M. Wang, Y. Yuan, M. Chuai, N. Chen, H. Hu, W. Chen, *Nano Lett.* **2022**, *22*, 3298–3306; b) W. Hu, J. Ju, N. Deng, M. Liu, W. Liu, Y. Zhang, L. Fan, W. Kang, B. Cheng, *J. Mater. Chem. A* **2021**, *9*, 25750–25772.
- [13] C. Li, L. Wang, J. Zhang, D. Zhang, J. Du, Y. Yao, G. Hong, *Energy Storage Mater.* **2022**, *44*, 104–135.
- [14] a) R. Chen, Q. Liu, L. Xu, X. Zuo, F. Liu, J. Zhang, X. Zhou, L. Mai, *ACS Energy Lett.* **2022**, *7*, 1719–1727; b) G. Ma, L. Miao, Y. Dong, W. Yuan, X. Nie, S. Di, Y. Wang, L. Wang, N. Zhang, *Energy Storage Mater.* **2022**, *47*,

- 203–210; c) X. Guo, G. Fang, W. Zhang, J. Zhou, L. Shan, L. Wang, C. Wang, T. Lin, Y. Tang, S. Liang, *Adv. Energy Mater.* **2018**, *8*, 1801819; d) N. Guo, W. Huo, X. Dong, Z. Sun, Y. Lu, X. Wu, L. Dai, L. Wang, H. Lin, H. Liu, H. Liang, Z. He, Q. Zhang, *Small Methods* **2022**, *6*, 2200597.
- [15] a) Z. Yu, Y. Cui, Z. Bao, *Cell Rep. Phys. Sci.* **2020**, *1*, 100119; b) J. Zheng, Z. Huang, F. Ming, Y. Zeng, B. Wei, Q. Jiang, Z. Qi, Z. Wang, H. Liang, *Small 2022*, *18*, 2200006; c) L. Xu, S. Tang, Y. Cheng, K. Wang, J. Liang, C. Liu, Y.-C. Cao, F. Wei, L. Mai, *Joule* **2018**, *2*, 1991–2015; d) Y. Xiao, Y. Wang, S.-H. Bo, J. C. Kim, L. J. Miara, G. Ceder, *Nat. Rev. Mater.* **2020**, *5*, 105–126.
- [16] D. Lin, Y. Liu, Y. Cui, *Nat. Nanotechnol.* **2017**, *12*, 194–206.
- [17] K. Qi, W. Zhu, X. Zhang, M. Liu, H. Ao, X. Wu, Y. Zhu, *ACS Nano* **2022**, *16*, 9461–9471.
- [18] A. Hu, F. Li, W. Chen, T. Lei, Y. Li, Y. Fan, M. He, F. Wang, M. Zhou, Y. Hu, Y. Yan, B. Chen, J. Zhu, J. Long, X. Wang, J. Xiong, *Adv. Energy Mater.* **2022**, *12*, 2202432.
- [19] a) M. D. Tikekar, L. A. Archer, D. L. Koch, *Sci. Adv.* **2016**, *2*, e1600320; b) Y. Lu, M. Tikekar, R. Mohanty, K. Hendrickson, L. Ma, L. A. Archer, *Adv. Energy Mater.* **2015**, *5*, 1402073.
- [20] E. Peled, S. Menkin, *J. Electrochem. Soc.* **2017**, *164*, A1703–A1719.
- [21] a) J. Tan, J. Matz, P. Dong, J. Shen, M. Ye, *Adv. Energy Mater.* **2021**, *11*, 2100046; b) A. Hu, W. Chen, X. Du, Y. Hu, T. Lei, H. Wang, L. Xue, Y. Li, H. Sun, Y. Yan, J. Long, C. Shu, J. Zhu, B. Li, X. Wang, J. Xiong, *Energy Environ. Sci.* **2021**, *14*, 4115–4124.
- [22] Y. Yang, C. Liu, Z. Lv, H. Yang, Y. Zhang, M. Ye, L. Chen, J. Zhao, C. C. Li, *Adv. Mater.* **2021**, *33*, 2007388.
- [23] L. Ma, Q. Li, Y. Ying, F. Ma, S. Chen, Y. Li, H. Huang, C. Zhi, *Adv. Mater.* **2021**, *33*, 2007406.
- [24] L. S. Cao, D. Li, T. Pollard, T. Deng, B. Zhang, C. Y. Yang, L. Chen, J. Vatamanu, E. Y. Hu, M. J. Hourwitz, L. Ma, M. Ding, Q. Li, S. Y. Hou, K. Gaskell, J. T. Fourkas, X. Q. Yang, K. Xu, O. Borodin, C. S. Wang, *Nat. Nanotechnol.* **2021**, *16*, 902–910.
- [25] J. Han, H. Euchner, M. Kuenzel, S. M. Hosseini, A. Groß, A. Varzi, S. Passerini, *ACS Energy Lett.* **2021**, *6*, 3063–3071.
- [26] Q. Jian, T. Wang, J. Sun, M. Wu, T. Zhao, *Energy Storage Mater.* **2022**, *53*, 559–568.
- [27] J. Y. Kim, G. Liu, R. E. A. Ardhi, J. Park, H. Kim, J. K. Lee, *Nano-Micro Lett.* **2022**, *14*, 46.
- [28] J. Hao, B. Li, X. Li, X. Zeng, S. Zhang, F. Yang, S. Liu, D. Li, C. Wu, Z. Guo, *Adv. Mater.* **2020**, *32*, 2003021.
- [29] X. Yang, C. Li, Z. Sun, S. Yang, Z. Shi, R. Huang, B. Liu, S. Li, Y. Wu, M. Wang, Y. Su, S. Dou, J. Sun, *Adv. Mater.* **2021**, *33*, 2105951.
- [30] P. Cao, X. Zhou, A. Wei, Q. Meng, H. Ye, W. Liu, J. Tang, J. Yang, *Adv. Funct. Mater.* **2021**, *31*, 2100398.
- [31] Q. Zhang, J. Luan, X. Huang, Q. Wang, D. Sun, Y. Tang, X. Ji, H. Wang, *Nat. Commun.* **2020**, *11*, 3961.
- [32] H. Neumann, G. Arlt, *Ferroelectrics* **1986**, *69*, 179–186.
- [33] P. Liang, J. Yi, X. Liu, K. Wu, Z. Wang, J. Cui, Y. Liu, Y. Wang, Y. Xia, J. Zhang, *Adv. Funct. Mater.* **2020**, *30*, 1908528.
- [34] M. Zhou, S. Guo, G. Fang, H. Sun, X. Cao, J. Zhou, A. Pan, S. Liang, *J. Energy Chem.* **2021**, *55*, 549–556.
- [35] H. Liu, J.-G. Wang, W. Hua, H. Sun, Y. Huyan, S. Tian, Z. Hou, J. Yang, C. Wei, F. Kang, *Adv. Sci.* **2021**, *8*, 2102612.
- [36] M. Liu, J. Cai, H. Ao, Z. Hou, Y. Zhu, Y. Qian, *Adv. Funct. Mater.* **2020**, *30*, 2004885.
- [37] H. Yan, S. Li, Y. Nan, S. Yang, B. Li, *Adv. Energy Mater.* **2021**, *11*, 2100186.
- [38] X. He, Y. Cui, Y. Qian, Y. Wu, H. Ling, H. Zhang, X.-Y. Kong, Y. Zhao, M. Xue, L. Jiang, L. Wen, *J. Am. Chem. Soc.* **2022**, *144*, 11168–11177.
- [39] H. Fan, M. Li, E. Wang, *Nano Energy* **2022**, *103*, 107751.
- [40] A. Chen, C. Zhao, Z. Guo, X. Lu, J. Zhang, N. Liu, Y. Zhang, N. Zhang, *Adv. Funct. Mater.* **2022**, *32*, 2203595.
- [41] X. Lu, C. Zhao, A. Chen, Z. Guo, N. Liu, L. Fan, J. Sun, N. Zhang, *Chem. Eng. J.* **2023**, *451*, 138772.
- [42] J.-L. Yang, J. Li, J.-W. Zhao, K. Liu, P. Yang, H. J. Fan, *Adv. Mater.* **2022**, *34*, 2202382.
- [43] L. T. Hieu, S. So, I. T. Kim, J. Hur, *Chem. Eng. J.* **2021**, *411*, 128584.
- [44] X. Liu, Q. Han, Q. Ma, Y. Wang, C. Liu, *Small* **2022**, *18*, 2203327.
- [45] H. Yan, C. Han, S. Li, J. Liu, J. Ren, S. Yang, B. Li, *Chem. Eng. J.* **2022**, *442*, 136081.
- [46] L. Kang, M. Cui, F. Jiang, Y. Gao, H. Luo, J. Liu, W. Liang, C. Zhi, *Adv. Energy Mater.* **2018**, *8*, 1801090.
- [47] Y. Liu, Y. Li, X. Huang, H. Cao, Q. Zheng, Y. Huo, J. Zhao, D. Lin, B. Xu, *Small* **2022**, *18*, 2203061.
- [48] B. Zhou, A. Hu, X. Zeng, M. He, R. Li, C. Zhao, Z. Yan, Y. Pan, J. Chen, Y. Fan, M. Liu, J. Long, *Chem. Eng. J.* **2022**, *450*, 137921.
- [49] H. Yang, Y. Qiao, Z. Chang, H. Deng, X. Zhu, R. Zhu, Z. Xiong, P. He, H. Zhou, *Adv. Mater.* **2021**, *33*, 2102415.
- [50] Z. Miao, F. Zhang, H. Zhao, M. Du, H. Li, H. Jiang, W. Li, Y. Sang, H. Liu, S. Wang, *Adv. Funct. Mater.* **2022**, *32*, 2111635.
- [51] M. He, C. Shu, A. Hu, R. Zheng, M. Li, Z. Ran, J. Long, *Energy Storage Mater.* **2022**, *44*, 452–460.
- [52] M. Liu, L. Yang, H. Liu, A. Amine, Q. Zhao, Y. Song, J. Yang, K. Wang, F. Pan, *ACS Appl. Mater. Interfaces* **2019**, *11*, 32046–32051.
- [53] X. Liu, F. Yang, W. Xu, Y. Zeng, J. He, X. Lu, *Adv. Sci.* **2020**, *7*, 2002173.
- [54] L. S. Cao, D. Li, T. Deng, Q. Li, C. S. Wang, *Angew. Chem. Int. Ed.* **2020**, *59*, 19292–19296; *Angew. Chem.* **2020**, *132*, 19454–19458.
- [55] S. Park, I. Kristanto, G. Y. Jung, D. B. Ahn, K. Jeong, S. K. Kwak, S. Y. Lee, *Chem. Sci.* **2020**, *11*, 11692–11698.
- [56] J. H. Park, M. J. Kwak, C. Hwang, K. N. Kang, N. Liu, J. H. Jang, B. A. Grzybowski, *Adv. Mater.* **2021**, *33*, 2101726.
- [57] Z. Zhao, R. Wang, C. Peng, W. Chen, T. Wu, B. Hu, W. Weng, Y. Yao, J. Zeng, Z. Chen, P. Liu, Y. Liu, G. Li, J. Guo, H. Lu, Z. Guo, *Nat. Commun.* **2021**, *12*, 6606.
- [58] J. Luo, C.-C. Fang, N.-L. Wu, *Adv. Energy Mater.* **2018**, *8*, 1701482.
- [59] T. Yim, S. H. Han, N. H. Park, M.-S. Park, J. H. Lee, J. Shin, J. W. Choi, Y. Jung, Y. N. Jo, J.-S. Yu, K. J. Kim, *Adv. Funct. Mater.* **2016**, *26*, 7817–7823.
- [60] K. Wu, J. Yi, X. Liu, Y. Sun, J. Cui, Y. Xie, Y. Liu, Y. Xia, J. Zhang, *Nano-Micro Lett.* **2021**, *13*, 79.
- [61] P. Zou, R. Zhang, L. Yao, J. Qin, K. Kisslinger, H. Zhuang, H. L. Xin, *Adv. Energy Mater.* **2021**, *11*, 2100982.
- [62] Y. Wang, T. Guo, J. Yin, Z. Tian, Y. Ma, Z. Liu, Y. Zhu, H. N. Alshareef, *Adv. Mater.* **2022**, *34*, 2106937.
- [63] S. Zhou, Y. Wang, H. Lu, Y. Zhang, C. Fu, I. Usman, Z. Liu, M. Feng, G. Fang, X. Cao, S. Liang, A. Pan, *Adv. Funct. Mater.* **2021**, *31*, 2104361.
- [64] Q. Yang, Y. Guo, B. Yan, C. Wang, Z. Liu, Z. Huang, Y. Wang, Y. Li, H. Li, L. Song, J. Fan, C. Zhi, *Adv. Mater.* **2020**, *32*, 2001755.
- [65] W. Li, K. Wang, M. Zhou, H. Zhan, S. Cheng, K. Jiang, *ACS Appl. Mater. Interfaces* **2018**, *10*, 22059–22066.
- [66] Z. Wang, J. Huang, Z. Guo, X. Dong, Y. Liu, Y. Wang, Y. Xia, *Joule* **2019**, *3*, 1289–1300.
- [67] H. Qin, W. Kuang, D. Huang, X. Zhang, J. Liu, L. Yi, F. Shen, Z. Wei, Y. Huang, J. Xu, H. He, *J. Mater. Chem. A* **2022**, *10*, 17440–17451.
- [68] L. Dong, W. Yang, W. Yang, H. Tian, Y. Huang, X. Wang, C. Xu, C. Wang, F. Kang, G. Wang, *Chem. Eng. J.* **2020**, *384*, 123355.
- [69] Y. Hao, J. Zhou, G. Wei, A. Liu, Y. Zhang, Y. Mei, B. Lu, M. Luo, M. Xie, *ACS Applied Energy Mater.* **2021**, *4*, 6364–6373.
- [70] N. Zhang, S. Huang, Z. Yuan, J. Zhu, Z. Zhao, Z. Niu, *Angew. Chem. Int. Ed.* **2021**, *60*, 2861–2865; *Angew. Chem.* **2021**, *133*, 2897–2901.
- [71] Z. Li, L. Wu, S. Dong, T. Xu, S. Li, Y. An, J. Jiang, X. Zhang, *Adv. Funct. Mater.* **2021**, *31*, 2006495.
- [72] a) C. Xie, Y. Li, Q. Wang, D. Sun, Y. Tang, H. Wang, *Carbon Energy* **2020**, *2*, 540–560; b) A. Bayaguud, Y. Fu, C. Zhu, *J. Energy Chem.* **2022**, *64*, 246–262.
- [73] Z. Cai, Y. Ou, J. Wang, R. Xiao, L. Fu, Z. Yuan, R. Zhan, Y. Sun, *Energy Storage Mater.* **2020**, *27*, 205–211.
- [74] J. B. Goodenough, Y. Kim, *Chem. Mater.* **2010**, *22*, 587–603.
- [75] Q. Li, L. Han, Q. Luo, X. Liu, J. Yi, *Batteries & Supercaps* **2022**, *5*, e202100417.
- [76] C. G. Morales-Guio, L.-A. Stern, X. Hu, *Chem. Soc. Rev.* **2014**, *43*, 6555–6569.
- [77] B. E. Conway, G. Jerkiewicz, *Electrochim. Acta* **2000**, *45*, 4075–4083.
- [78] D. Han, S. Wu, S. Zhang, Y. Deng, C. Cui, L. Zhang, Y. Long, H. Li, Y. Tao, Z. Weng, Q.-H. Yang, F. Kang, *Small* **2020**, *16*, 2001736.
- [79] P. Xiao, H. Li, J. Fu, C. Zeng, Y. Zhao, T. Zhai, H. Li, *Energy Environ. Sci.* **2022**, *15*, 1638–1646.
- [80] L. Wang, W. Huang, W. Guo, Z. H. Guo, C. Chang, L. Gao, X. Pu, *Adv. Funct. Mater.* **2022**, *32*, 2108533.
- [81] W. Huang, L. Wang, Q. Zhu, P. Zhang, X. Pu, L. Gao, *Mater. Today Commun.* **2022**, *33*, 104576.
- [82] K. Zhao, C. Wang, Y. Yu, M. Yan, Q. Wei, P. He, Y. Dong, Z. Zhang, X. Wang, L. Mai, *Adv. Mater. Interfaces* **2018**, *5*, 1800848.
- [83] H. He, H. Tong, X. Song, X. Song, J. Liu, J. Mater. Chem. A **2020**, *8*, 7836–7846.
- [84] Z. Zhao, J. Zhao, Z. Hu, J. Li, J. Li, Y. Zhang, C. Wang, G. Cui, *Energy Environ. Sci.* **2019**, *12*, 1938–1949.
- [85] J. Hao, X. Li, S. Zhang, F. Yang, X. Zeng, S. Zhang, G. Bo, C. Wang, Z. Guo, *Adv. Funct. Mater.* **2020**, *30*, 2001263.

- [86] E. McCafferty, *Introduction to Corrosion Science*[M]. Springer New York. 2010.
- [87] D. Li, L. Cao, T. Deng, S. Liu, C. Wang, *Angew. Chem. Int. Ed. Engl.* **2021**, *60*, 13035–13041.
- [88] W. Guo, X. Bai, Z. Cong, C. Pan, L. Wang, L. Li, C. Chang, W. Hu, X. Pu, *ACS Appl. Mater. Interfaces* **2022**, *14*, 41988–41996.
- [89] P. Zou, D. Nykypanchuk, G. Doerk, H. L. Xin, *ACS Appl. Mater. Interfaces* **2021**, *13*, 60092–60098.
- [90] D. Lee, H.-I. Kim, W.-Y. Kim, S.-K. Cho, K. Baek, K. Jeong, D. B. Ahn, S. Park, S. J. Kang, S.-Y. Lee, *Adv. Funct. Mater.* **2021**, *31*, 2103850.
- [91] Z. Chang, H. Yang, Y. Qiao, X. Zhu, P. He, H. Zhou, *Adv. Mater.* **2022**, *34*, 2201339.
- [92] X. Xie, S. Liang, J. Gao, S. Guo, J. Guo, C. Wang, G. Xu, X. Wu, G. Chen, J. Zhou, *Energy Environ. Sci.* **2020**, *13*, 503–510.
- [93] Y. Cui, Q. Zhao, X. Wu, X. Chen, J. Yang, Y. Wang, R. Qin, S. Ding, Y. Song, J. Wu, K. Yang, Z. Wang, Z. Mei, Z. Song, H. Wu, Z. Jiang, G. Qian, L. Yang, F. Pan, *Angew. Chem. Int. Ed. Engl.* **2020**, *59*, 16594–16601.
- [94] P. Wang, S. Liang, C. Chen, X. Xie, J. Chen, Z. Liu, Y. Tang, B. Lu, J. Zhou, *Adv. Mater.* **2022**, *34*, 2202733.
- [95] H. Ooka, J. Huang, K. S. Exner, *Front. Energy Res.* **2021**, *9*, 654460.
- [96] Y. Sui, X. Ji, *Chem. Rev.* **2021**, *121*, 6654–6695.
- [97] Y. Zheng, Y. Jiao, Y. Zhu, L. H. Li, Y. Han, Y. Chen, M. Jaroniec, S.-Z. Qiao, *J. Am. Chem. Soc.* **2016**, *138*, 16174–16181.
- [98] L. Ma, C. Zhi, *Electrochim. Commun.* **2021**, *122*, 106898.
- [99] C. Zhao, Y. Du, Z. Guo, A. Chen, N. Liu, X. Lu, L. Fan, Y. Zhang, N. Zhang, *Energy Storage Mater.* **2022**, *53*, 322–330.
- [100] C. Guo, J. Zhou, Y. Chen, H. Zhuang, Q. Li, J. Li, X. Tian, Y. Zhang, X. Yao, Y. Chen, S. L. Li, Y. Q. Lan, *Angew. Chem. Int. Ed. Engl.* **2022**, *61*, e202210871.
- [101] J. Barton and J. Bockris, *Proc. R. Soc. London Ser. A* **1997**, *268*, 485–505.
- [102] J. W. Diggle, A. R. Despic, J. O. M. Bockris, *J. Electrochem. Soc.* **1969**, *116*, 1503.
- [103] I. Yoshimatsu, T. Hirai, J. i. Yamaki, *J. Electrochem. Soc.* **1988**, *135*, 2422–2427.
- [104] C. Monroe, J. Newman, *J. Electrochem. Soc.* **2004**, *151*, A880-A886.
- [105] Z. Hong, Z. Ahmad, V. Viswanathan, *ACS Energy Lett.* **2020**, *5*, 2466–2474.
- [106] H. Qiu, X. Du, J. Zhao, Y. Wang, J. Ju, Z. Chen, Z. Hu, D. Yan, X. Zhou, G. Cui, *Nat. Commun.* **2019**, *10*, 5374.
- [107] H. Jiang, H. Peng, H. Guo, Y. Zeng, L. Li, Y. Zhang, Y. Chen, X. Chen, J. Zhang, R. Chu, *ACS Appl. Mater. Interfaces* **2020**, *12*, 51344–51356.
- [108] X. Fan, X. Ji, F. Han, J. Yue, J. Chen, L. Chen, T. Deng, J. Jiang, C. Wang, *Sci. Adv.* **2018**, *4*, eaau9245.
- [109] Y. Chu, S. Zhang, S. Wu, Z. Hu, G. Cui, J. Luo, *Energy Environ. Sci.* **2021**, *14*, 3609–3620.
- [110] Y. Zhang, C. Peng, Y. Zhang, S. Yang, Z. Zeng, X. Zhang, L. Qie, L.-L. Zhang, Z. Wang, *Chem. Eng. J.* **2022**, *448*, 137653.
- [111] R. Zhao, Y. Yang, G. Liu, R. Zhu, J. Huang, Z. Chen, Z. Gao, X. Chen, L. Qie, *Adv. Funct. Mater.* **2021**, *31*, 2001867.
- [112] Q. Jian, Y. Wan, Y. Lin, M. Ni, M. Wu, T. Zhao, *ACS Appl. Mater. Interfaces* **2021**, *13*, 52659–52669.
- [113] H. Du, R. Zhao, Y. Yang, Z. Liu, L. Qie, Y. Huang, *Angew. Chem. Int. Ed.* **2022**, *61*, e202114789.
- [114] a) S. Huang, F. Wan, S. Bi, J. Zhu, Z. Niu, J. Chen, *Angew. Chem. Int. Ed. Engl.* **2019**, *58*, 4313–4317; b) J. Liu, J. Long, Z. Shen, X. Jin, T. Han, T. Si, H. Zhang, *Adv. Sci.* **2021**, *8*, 2004689.
- [115] G. Zheng, C. Wang, A. Pei, J. Lopez, F. Shi, Z. Chen, A. D. Sendek, H.-W. Lee, Z. Lu, H. Schneider, M. M. Safont-Sempere, S. Chu, Z. Bao, Y. Cui, *ACS Energy Lett.* **2016**, *1*, 1247–1255.
- [116] X. Kong, P. E. Rudnicki, S. Choudhury, Z. Bao, J. Qin, *Adv. Funct. Mater.* **2020**, *30*, 1910138.
- [117] S. Wei, Z. Cheng, P. Nath, M. D. Tikekar, G. Li, L. A. Archer, *Sci. Adv.* **2018**, *4*, eaao6243.
- [118] Z. Guo, L. Fan, C. Zhao, A. Chen, N. Liu, Y. Zhang, N. Zhang, *Adv. Mater.* **2022**, *34*, 2105133.
- [119] J. Zhou, M. Peng, X. Xia, S. Qian, Z. Wang, C. Zhu, X. Zeng, H. Ji, S. Wang, X. Zhou, J. Liu, X. Shen, Y. Cheng, T. Qian, C. Yan, *Nano Lett.* **2022**, *22*, 2898–2906.
- [120] H. Dong, X. Hu, G. He, *Nanoscale* **2022**, *14*, 14544–14551.
- [121] W. Cao, Q. Li, X. Yu, H. Li, *eScience* **2022**, *2*, 47–78.

Manuscript received: October 27, 2022
 Revised manuscript received: November 21, 2022
 Accepted manuscript online: November 23, 2022
 Version of record online: December 12, 2022